

## A Mathematical Model for SAR Imaging beyond the First Born Approximation\*

Mikhail Gilman<sup>†</sup> and Semyon Tsynkov<sup>‡</sup>

**Abstract.** The assumption of weak scattering is standard for the mathematical analysis of synthetic aperture radar (SAR), as it helps linearize the inverse problem via the first Born approximation and thus makes it amenable to solution. Yet it is not consistent with another common assumption, that the interrogating waves do not penetrate into the target material and get scattered off its surface only, which essentially means that the scattering is strong. In the paper, we revisit the foundations of the SAR ambiguity theory in order to address this and other existing inconsistencies, such as the absence of the Bragg scale in scattering. We introduce a new model for radar targets that allows us to compute the scattered field from first principles. This renders the assumption of weak scattering unnecessary yet keeps the overall inverse scattering problem linear. Finally, we show how one can incorporate the Leontovich boundary condition into SAR ambiguity theory.

**Key words.** synthetic aperture imaging, SAR ambiguity theory, linearized scattering, linearized inverse problem, backscattering, Bragg resonance, weak scattering, strong scattering

**AMS subject classifications.** 35B20, 35R30, 45Q05, 78A40, 78A45, 78A46, 78A55, 78M34, 78M35, 86A22, 94A08, 94A12

**DOI.** 10.1137/140973025

**1. Introduction.** In synthetic aperture radar (SAR) ambiguity theory (see [5, 6, 8]) the image is represented as a convolution of the target (ground) reflectivity  $\nu(\mathbf{z})$  with the imaging kernel  $W(\mathbf{y}, \mathbf{z}) = W(\mathbf{y} - \mathbf{z})$  that characterizes the radar system:

$$(1.1) \quad I(\mathbf{y}) = \int \nu(\mathbf{z})W(\mathbf{y}, \mathbf{z})d\mathbf{z}.$$

Representation (1.1) is useful as it allows for a rigorous mathematical analysis of the image properties, particularly its resolution. Indeed, in the ideal case, where  $W(\mathbf{y}, \mathbf{z}) = \delta(\mathbf{y} - \mathbf{z})$ , the image  $I(\mathbf{y})$  exactly coincides with the unknown ground reflectivity  $\nu(\mathbf{z})$ . In real-world situations, though, the kernel  $W(\mathbf{y}, \mathbf{z})$  (often referred to as the generalized ambiguity function; see section 2.1) is never equal to the  $\delta$ -function, and hence the imperfections of the image can be unambiguously attributed to the properties of the kernel. However, the assumptions that are typically made when deriving formula (1.1) may be inconsistent.

First and foremost, linearity with respect to  $\nu$  of the inverse problem of reconstructing the unknown reflectivity from the received radar signals (scattered off the target) is its key

---

\*Received by the editors June 16, 2014; accepted for publication (in revised form) November 21, 2014; published electronically January 22, 2015. This work was supported by the US Air Force Office of Scientific Research (AFOSR) under agreements FA9550-10-1-0092 and FA9550-14-1-0218.

<http://www.siam.org/journals/siims/8-1/97302.html>

<sup>†</sup>Department of Mathematics, North Carolina State University, Box 8205, Raleigh, NC 27695 ([mgilman@ncsu.edu](mailto:mgilman@ncsu.edu), <http://www4.ncsu.edu/~mgilman/>).

<sup>‡</sup>Corresponding author. Department of Mathematics, North Carolina State University, Raleigh, NC 27695, and Moscow Institute of Physics and Technology, Dolgoprudny, 141700, Russia ([tsynkov@math.ncsu.edu](mailto:tsynkov@math.ncsu.edu), <http://www4.ncsu.edu/~stsynkov/>).

property that enables a solution in the form of (1.1). The linearity is normally attained by assuming that the scattering is weak and employing the first Born approximation [3, section 13.1.2]. Equivalently, it means that the variations of the scattering medium on top of the constant vacuum background are small, so that the scattered field can be considered a first order perturbation of the incident field that propagates in free space with no obstructions. These considerations are standard in the mathematical literature on SAR, including our own work [14, 13, 15, 26, 29]. However, they are inconsistent with the most common SAR imaging scenario in which the scattering occurs only on the surface of the target so that convolution (1.1) effectively becomes two-dimensional. In this case, the radar signals do not penetrate into the target, which implies that the scattering is strong rather than weak.

An additional issue in the conventional SAR ambiguity theory that may be deemed problematic is the expression of the ground reflectivity  $\nu$  as a function of the local refraction index only (see formulae (2.11') and (2.12') in section 2.1). It is well known, for example, that in this case a homogeneous dielectric half-space yields only specular (i.e., mirror-like) reflection, which makes the monostatic SAR imaging impossible. At the same time, to the best of our knowledge the Bragg-type resonant scattering mechanism has not yet been incorporated into the SAR ambiguity theory. It is this mechanism that enables scattering back toward the emitting antenna, provided that a certain spatial scale is present in the spectrum of inhomogeneities of the refraction index; see section 3.3.

The main objective of the current paper is to generalize the conventional SAR ambiguity theory and remove the foregoing inconsistencies. Its key new result is the construction of an alternative mathematical model for distributed radar targets that still allows one to preserve the standard representation (1.1) for the image yet avoids the assumption of weak scattering (along with the first Born approximation) and does not employ singular ground reflectivity functions.

Our new model for radar targets enables computing the scattered field from first principles. Specifically, the scattering medium itself, which is a horizontally inhomogeneous dielectric half-space, is introduced in the beginning of section 3 and then further delineated in the beginning of section 3.2; see (3.4). The computation of the scattered field is based on the separation of variables, which is rendered by Fourier transforms in time and in space. The resulting scattered field is given by (3.46) and (3.47).

While not assuming that the scattering is weak, the new model keeps the overall inverse scattering problem linear with respect to the material characteristics, which yields the solution in the form of convolution (1.1). In essence, the model still employs linearization, but against a different background solution, not necessarily the unobstructed incident field in free space. Yet when the scattering is indeed weak, the new constructs transform into the previous ones. In other words, in the case of weak scattering the linearization is performed against the aforementioned free space incident solution. This is fully equivalent to using the first Born approximation, as done in earlier studies of the SAR ambiguity theory. The discussion in the current paper is restricted to the scalar framework. Yet the model and the methodology that we introduce here also allow one to analyze effects related to polarization. This will be done in the future.

In the literature on inverse problems, there are other approaches that avoid the assumption of weak scattering and the first Born approximation. Among the most recent advances are

the linear sampling method [4] and the factorization method [19]. Those two methods allow for strong as opposed to weak scattering and are used predominantly for solving the shape reconstruction problem in the frequency domain. To the best of our knowledge, ideas similar to those of [4, 19] have not been applied to SAR imaging.

Hereafter, we analyze the most general setting for the scattering of radar signals off the target; i.e., we consider two arbitrary directions for the incident and scattered waves. As for the SAR imaging scenario, for simplicity we restrict ourselves to a monostatic<sup>1</sup> narrow-band stripmap imaging, as in [5, 8], with a small aperture angle. Unlike in [13, 14, 15, 26, 29], the signal propagation is considered nondispersive. Other assumptions are introduced as needed.

The paper is organized as follows. In section 2, we present an account of conventional SAR ambiguity theory and discuss its deficiencies; this section also refers to Appendix A for technical derivations. In section 3, we present a new, more general, model for SAR targets that exploits a horizontally inhomogeneous material half-space and allows us to overcome the difficulties that characterize the conventional theory. An alternative (less rigorous) model based on the Leontovich boundary condition is briefly discussed in Appendix B. In section 4, we generalize the conventional SAR ambiguity theory using the new scattering model of section 3. Finally, in section 5, we outline our conclusions and discuss future work.

## 2. Revisiting the SAR ambiguity theory.

**2.1. Conventional approach.** In the framework of the conventional SAR ambiguity theory (see [5, 6, 8]), the radar signals are interpreted as scalar quantities. Their propagation in free space is governed by the d'Alembert equation:

$$(2.1) \quad \left( \frac{1}{c^2} \frac{\partial^2}{\partial t^2} - \Delta \right) u = f,$$

where  $\Delta$  is the Laplacian,  $c$  is the speed of light, and  $f = f(t, \mathbf{z})$  is the source,  $\mathbf{z} \in \mathbb{R}^3$ .

For an unsteady point source (emitting radar antenna) located at a fixed  $\mathbf{x} \in \mathbb{R}^3$ ,

$$f(t, \mathbf{z}) = P(t)\delta(\mathbf{z} - \mathbf{x}),$$

the solution of (2.1) is given by the standard retarded potential,

$$(2.2) \quad u^{(0)}(t, \mathbf{z}) = \frac{1}{4\pi} \frac{P(t - |\mathbf{z} - \mathbf{x}|/c)}{|\mathbf{z} - \mathbf{x}|}.$$

Hereafter, solution (2.2) will be used in the capacity of the incident field.

In [5, 8], the terrain to be imaged is characterized by the refraction index  $n = n(\mathbf{z})$ . Then, the total field  $u = u^{(0)} + u^{(1)}$  is governed by the variable coefficient wave equation:

$$(2.3) \quad \left( \frac{1}{v^2(\mathbf{z})} \frac{\partial^2}{\partial t^2} - \Delta \right) (u^{(0)} + u^{(1)}) = f,$$

where  $u^{(1)} = u^{(1)}(t, \mathbf{z})$  is the scattered field and  $v(\mathbf{z}) = \frac{c}{n(\mathbf{z})}$  is the speed of light in the material. In the vacuum region, it is assumed that  $n(\mathbf{z}) = 1$ , so that  $v(\mathbf{z}) = c$  and (2.3)

---

<sup>1</sup>The emitting and receiving antennas are at the same location; it may be one and the same antenna.

transforms back to (2.1). Subtracting the constant coefficient equation (2.1) written for the incident field  $u^{(0)}$  on the entire space  $\mathbb{R}^3$  from the variable coefficient equation (2.3), we have

$$(2.4) \quad \left( \frac{1}{c^2} \frac{\partial^2}{\partial t^2} - \Delta \right) u^{(1)} = \frac{1 - n^2(\mathbf{z})}{c^2} \frac{\partial^2}{\partial t^2} (u^{(0)} + u^{(1)}).$$

Equation (2.4) involves no simplifying assumptions, and its solution  $u^{(1)}$  is the same as one would have obtained by solving (2.3) with  $u^{(0)}$  found from (2.1). Hence, this linear variable coefficient partial differential equation can be used for direct computation of the scattered field  $u^{(1)}$  if the incident field  $u^{(0)}$  and the refraction index  $n(\mathbf{z})$  are given.

However, the central problem of SAR imaging is the inverse problem of reconstructing the unknown material parameter  $n(\mathbf{z})$ , given the incident field  $u^{(0)}$  and taking the scattered field  $u^{(1)}$  as the observable data. It is very important to realize, though, that whereas the incident field  $u^{(0)}$  is known on the entire  $\mathbb{R}^3$ , the scattered field  $u^{(1)}$  can be considered known only at certain locations away from the target region.<sup>2</sup> Thus, the inverse problem of SAR imaging becomes effectively nonlinear, because on the right-hand side of (2.4) the unknown quantity of interest,  $n(\mathbf{z})$ , is multiplied by another unknown quantity,  $u^{(1)}(t, \mathbf{z})$ .

The most common assumption made in the SAR literature in order to simplify the formulation of the inverse problem is that of weak scattering:

$$(2.5) \quad |n(\mathbf{z}) - 1| \ll 1, \quad |u^{(1)}| \ll |u^{(0)}|.$$

Relations (2.5) allow one to employ the first Born approximation [3, section 13.1.2] and linearize (2.4) by disregarding  $u^{(1)}$  on its right-hand side. This linearization yields an inhomogeneous d'Alembert equation for the scattered field:

$$(2.6) \quad \left( \frac{1}{c^2} \frac{\partial^2}{\partial t^2} - \Delta \right) u^{(1)} = \frac{1 - n^2(\mathbf{z})}{c^2} \frac{\partial^2 u^{(0)}}{\partial t^2}.$$

The source term on the right-hand side of (2.6) is due to the incident field  $u^{(0)}(t, \mathbf{z})$  of (2.2) and variable refraction index  $n(\mathbf{z})$ . Solution to (2.6) is given by the Kirchhoff integral:

$$(2.7) \quad u^{(1)}(t, \mathbf{x}') = \frac{1}{4\pi} \int \frac{1 - n^2(\mathbf{z})}{|\mathbf{x}' - \mathbf{z}|c^2} \frac{\partial^2 u^{(0)}}{\partial t^2} \left( t - \frac{|\mathbf{x}' - \mathbf{z}|}{c}, \mathbf{z} \right) d\mathbf{z},$$

where  $\mathbf{x}'$  can be an arbitrary point in  $\mathbb{R}^3$ . One can think of  $\mathbf{x}'$  as the location of the receiving antenna. For monostatic SAR, it coincides with that of the emitting antenna,  $\mathbf{x}' = \mathbf{x}$ .

Hereafter, we will consider the emitted signal in the form of a linear chirp (frequency-modulated pulse) with the central carrier frequency  $\omega_0$ :

$$(2.8) \quad P(t) = A(t)e^{-i\omega_0 t}, \quad \text{where } A(t) = \chi_\tau(t)e^{-iat^2}$$

and

$$(2.9) \quad \chi_\tau(t) = \begin{cases} 1, & t \in [-\tau/2, \tau/2], \\ 0, & \text{otherwise.} \end{cases}$$

---

<sup>2</sup>In practice,  $u^{(1)}$  is known as the receiving radar antenna, which is mounted on an airborne or spaceborne platform located above the imaged terrain (Earth's surface); see Figure 1.

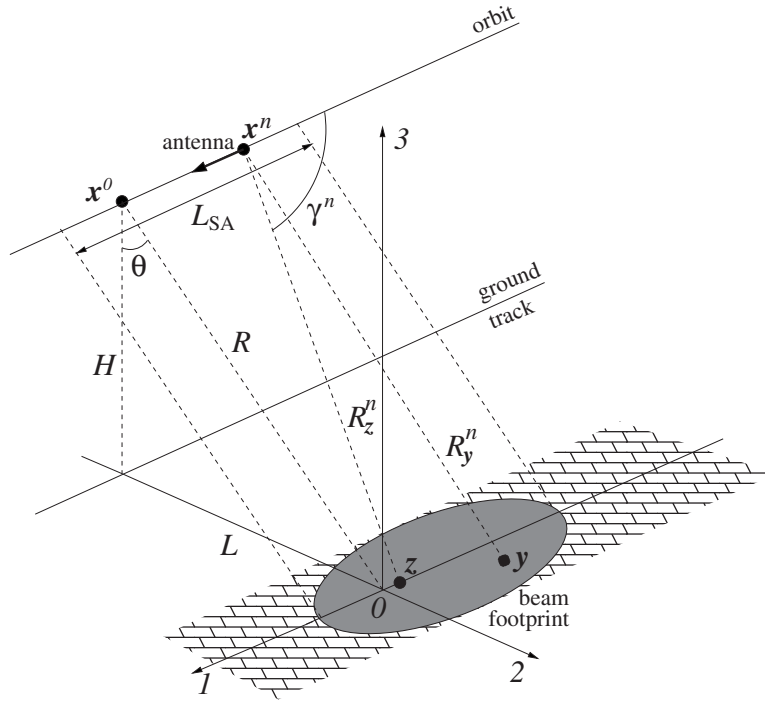


**Figure 1.** Schematic for the monostatic broadside stripmap SAR imaging.  $H$  is the orbit altitude,  $L$  is the distance (range) from the ground track to the target, and  $R$  is the slant range.

In (2.8),  $\alpha = \frac{B}{2\tau}$  is the chirp rate,  $\frac{B}{2\pi}$  is the bandwidth of the chirp ( $B \ll \omega_0$ ), and  $\tau$  is its duration. The amplitude  $A(t)$  in (2.8) is supposed to vary slowly compared to the fast oscillation  $e^{-i\omega_0 t}$ . Hence, it can be left out when differentiating the incident field (2.2) for substitution into (2.6), which yields

$$(2.10) \quad \frac{\partial^2 u^{(0)}}{\partial t^2}(t, \mathbf{z}) \approx -\omega_0^2 u^{(0)}(t, \mathbf{z}) = -\frac{\omega_0^2}{4\pi} \frac{P(t - |\mathbf{z} - \mathbf{x}|/c)}{|\mathbf{z} - \mathbf{x}|}.$$

Consequently, from (2.7) we have

$$(2.11) \quad u^{(1)}(t, \mathbf{x}') \approx \int \nu(\mathbf{z}, \mathbf{x}, \mathbf{x}') P(t - |\mathbf{x} - \mathbf{z}|/c - |\mathbf{x}' - \mathbf{z}|/c) dz,$$

where

$$(2.12) \quad \nu(\mathbf{z}, \mathbf{x}, \mathbf{x}') = -\frac{\omega_0^2}{16\pi^2 |\mathbf{z} - \mathbf{x}| |\mathbf{z} - \mathbf{x}'|} \frac{1 - n^2(\mathbf{z})}{c^2}.$$

For typical SAR geometries, the distance between either of the antennas,  $\mathbf{x}$  or  $\mathbf{x}'$ , and the target is much larger than the resolution scale at the target, which can be considered a typical variation of  $\mathbf{z}$  (a schematic for the monostatic ( $\mathbf{x} = \mathbf{x}'$ ) broadside imaging is shown in Figure 1). Moreover, this distance is also much larger than the length of the synthetic aperture, which can be considered a typical variation of either  $\mathbf{x}$  or  $\mathbf{x}'$ . Given that the

quantity  $1 - n^2(\mathbf{z})$  on the right-hand side of (2.12) is already small due to the first relation of (2.5), one can disregard the dependence of the denominator in formula (2.12) on any of the variables  $\mathbf{z}$ ,  $\mathbf{x}$ , or  $\mathbf{x}'$ , i.e., interpret it as a constant. Indeed, taking the variation of the denominator into account would bring along a correction proportional to the product of two small terms, which does not need to be considered in the context of the Born linearization (see also [5, section 3]).

Consequently, we can replace (2.11) and (2.12) with

$$(2.11') \quad u^{(1)}(t, \mathbf{x}') \approx \int \nu(\mathbf{z}) P(t - |\mathbf{x} - \mathbf{z}|/c - |\mathbf{x}' - \mathbf{z}|/c) d\mathbf{z}$$

and

$$(2.12') \quad \nu(\mathbf{z}) = -\frac{\omega_0^2}{16\pi^2 R^2} \frac{1 - n^2(\mathbf{z})}{c^2},$$

respectively, where  $R$  is the distance (slant range) between the SAR platform trajectory (e.g., satellite orbit) and the target; see Figure 1. The reflectivity coefficient  $\nu(\mathbf{z})$  in (2.11'), (2.12') therefore becomes a function of the local index of refraction  $n(\mathbf{z})$  only.

For the remainder of this section, we will discuss how the foregoing linearized model based on weak scattering can be used for the analysis of SAR imaging. In doing so, we will consider only the case of a monostatic SAR, i.e.,  $\mathbf{x}' = \mathbf{x}$ . Then, (2.11') becomes

$$(2.11'') \quad u^{(1)}(t, \mathbf{x}) \approx \int \nu(\mathbf{z}) P(t - 2|\mathbf{x} - \mathbf{z}|/c) d\mathbf{z}.$$

Solving the inverse scattering problem for SAR would mean obtaining  $\nu(\mathbf{z})$  from the known  $u^{(1)}(t, \mathbf{x})$ . In other words, one needs to invert the integral operator that acts on  $\nu(\mathbf{z})$  on the right-hand side of (2.11''). The approximate inversion is done by first applying the matched filter  $\overline{P(t - 2|\mathbf{y} - \mathbf{x}|/c)}$  to the received antenna signal  $u^{(1)}(t, \mathbf{x})$  of (2.11'')

$$(2.13) \quad \begin{aligned} I_{\mathbf{x}}(\mathbf{y}) &= \int_{\chi} \overline{P(t - 2R_{\mathbf{y}}/c)} u^{(1)}(t, \mathbf{x}) dt \\ &= \int d\mathbf{z} \nu(\mathbf{z}) \underbrace{\int_{\chi} dt \overline{P(t - 2R_{\mathbf{y}}/c)} P(t - 2R_{\mathbf{z}}/c)}_{W_{\mathbf{x}}(\mathbf{y}, \mathbf{z})}, \end{aligned}$$

where we have introduced

$$(2.14) \quad R_{\mathbf{y}} = |\mathbf{y} - \mathbf{x}| \quad \text{and} \quad R_{\mathbf{z}} = |\mathbf{z} - \mathbf{x}|.$$

In (2.13), the overbar denotes the complex conjugate, the interior integral  $W_{\mathbf{x}}(\mathbf{y}, \mathbf{z})$  is the point spread function (PSF), and the notation  $\int_{\chi}$  means that the integration limits are determined by the indicator function(s)  $\chi_{\tau}$  under the integral; see (2.8) and (2.9). The image  $I_{\mathbf{x}}$  for a single pulse emitted from the point  $\mathbf{x}$  is thus given by

$$(2.15) \quad I_{\mathbf{x}}(\mathbf{y}) = \int W_{\mathbf{x}}(\mathbf{y}, \mathbf{z}) \nu(\mathbf{z}) d\mathbf{z}.$$

The next stage of inversion is to consider a sequence of radar pulses emitted at times  $t_n$  from the equally spaced positions  $\mathbf{x}^n$ ,  $-N/2 \leq n \leq N/2$ , as the antenna moves along the linear flight path (orbit). We will assume that the  $n$ th pulse is emitted, and the scattered response received, when the antenna is at a standstill at the position  $\mathbf{x}^n$ , after which it moves to the next emitting/receiving position. This simplified treatment is known as the start-stop approximation; it is commonly used in the SAR literature; see, e.g., [5, 6]. The applicability of this approximation to rapidly moving platforms (satellites) is analyzed in [30].

Note that a real-life radar antenna is not a point source and does not emit spherically symmetric waves. It rather emits a beam, which has the same functional dependence (2.2),<sup>3</sup> but is confined to a narrow angular width (see [14, Table 1]). Hereafter, we assume that the pulses (beams) are emitted toward the ground in the direction normal to the platform trajectory. This corresponds to the broadside stripmap SAR imaging; see Figure 1. In [30], we also show that a nonzero squint angle (the angle between the direction of the beam and the normal to the trajectory) can be introduced without much additional effort.

The range of  $\mathbf{x}^n$  for  $n = -N/2, \dots, N/2$  defines the synthetic aperture of length  $L_{SA}$ . Given a location on the ground, this range consists of those  $\mathbf{x}^n$  for which this location remains within the footprint of the antenna beam; see Figure 1. The full image  $I(\mathbf{y})$  is a coherent sum of  $I_{\mathbf{x}^n}(\mathbf{y})$  given by (2.15) for  $\mathbf{x} = \mathbf{x}^n$ :

$$(2.16) \quad I(\mathbf{y}) = \sum_{n=-N/2}^{N/2} \int W_{\mathbf{x}^n}(\mathbf{y}, \mathbf{z}) \nu(\mathbf{z}) d\mathbf{z} = \int W(\mathbf{y}, \mathbf{z}) \nu(\mathbf{z}) d\mathbf{z} = W * \nu,$$

where  $\mathbf{x}^n$  is the location of the antenna at the physical moment of time  $t_n$  and  $n = -N/2, \dots, N/2$  is often referred to as the “slow time” in the SAR literature; see, e.g., [6, Chapter 9]. Accordingly, the function  $W(\mathbf{y}, \mathbf{z})$  in (2.16) is obtained by summing up all the PSFs  $W_{\mathbf{x}^n}(\mathbf{y}, \mathbf{z})$ :

$$(2.17) \quad \begin{aligned} W(\mathbf{y}, \mathbf{z}) &= \sum_{n=-N/2}^{N/2} \int_{\mathcal{X}} dt \overline{P(t - t_n - 2R_{\mathbf{y}}^n/c)} P(t - t_n - 2R_{\mathbf{z}}^n/c) \\ &= \sum_{n=-N/2}^{N/2} \int_{\mathcal{X}} dt \overline{A(t - t_n - 2R_{\mathbf{y}}^n/c)} A(t - t_n - 2R_{\mathbf{z}}^n/c) e^{2i\omega_0(R_{\mathbf{z}}^n/c - R_{\mathbf{y}}^n/c)}, \end{aligned}$$

where

$$(2.18) \quad R_{\mathbf{y}}^n = |\mathbf{y} - \mathbf{x}^n| \quad \text{and} \quad R_{\mathbf{z}}^n = |\mathbf{z} - \mathbf{x}^n|.$$

$W(\mathbf{y}, \mathbf{z})$  of (2.17) is called the generalized ambiguity function (GAF). Due to the integral representation (2.16),  $W(\mathbf{y}, \mathbf{z}_0)$  for a given  $\mathbf{z}_0$  can formally be thought of as the image  $I(\mathbf{y})$  of a point source  $\nu(\mathbf{z}) = \delta(\mathbf{z} - \mathbf{z}_0)$ . It will subsequently be shown<sup>4</sup> that  $W$  can be expressed

<sup>3</sup>The standard retarded potential (2.2) represents radiation of waves by a stationary source; it can be used for describing the SAR pulses because of the start-stop approximation. Radiation of waves by moving sources is described by Liénard–Wiechert potentials [20, Chapter 8]. In the case of a straightforward uniform motion, the solution can also be obtained using Lorentz transform, which was done in [30] for analyzing SAR.

<sup>4</sup>See the discussion at the end of this section, right after (2.26).

as  $W(\mathbf{y}, \mathbf{z}) = W(\mathbf{y} - \mathbf{z})$ , which justifies the convolution notation  $W * \nu$  for the integral (2.16). Note that (1.1) for the image, which is discussed in section 1, coincides with (2.16).

As the matched filter is given by the complex conjugate of  $P(\cdot)$  (see (2.13)), the foregoing approximate inversion of the integral operator on the right-hand side of (2.11'') corresponds to applying the formal adjoint operator. The reason is that if the direct operator in (2.11'') were a genuine Fourier transform of  $\nu(\mathbf{z})$ , then its adjoint would have been the same as its inverse. However, neither of the operators is equivalent to a true Fourier transform (see the definition of  $P(\cdot)$  in (2.8), (2.9)), and hence the inversion is only approximate rather than exact. In other words, the kernel  $W$  is not a  $\delta$ -function,  $W(\mathbf{y} - \mathbf{z}) \neq \delta(\mathbf{y} - \mathbf{z})$ , and the image  $I(\mathbf{y})$  does not, generally speaking, coincide with  $\nu(\mathbf{z})$ ; see Appendix A for additional detail.

To quantify the discrepancies between the image  $I(\mathbf{y})$  and the reflectivity  $\nu(\mathbf{z})$ , one needs to analyze the properties of the imaging kernel  $W(\mathbf{y}, \mathbf{z})$ . We first notice that in each individual term of the sum (2.17),  $t - t_n$  can be replaced with  $t$  by merely changing the integration variable. The remaining dependence of  $\overline{A(t - 2R_{\mathbf{y}}^n/c)}$  and  $A(t - 2R_{\mathbf{z}}^n/c)$  on  $n$  is through  $\mathbf{x}^n$  (see (2.18)); it is weak because  $A$  in (2.8) is a slowly varying envelope itself. Hence, we can take  $\overline{A(\cdot)}$  and  $A(\cdot)$  out of the summation over  $n$ , so that the GAF  $W(\mathbf{y}, \mathbf{z})$  of (2.17) can approximately be represented as a product of two factors (see, e.g., [5, 8, 26]):

$$(2.19) \quad W(\mathbf{y}, \mathbf{z}) \approx W_{\Sigma}(\mathbf{y}, \mathbf{z}) \cdot W_{\text{R}}(\mathbf{y}, \mathbf{z}),$$

where

$$(2.20) \quad W_{\Sigma}(\mathbf{y}, \mathbf{z}) = \sum_{n=-N/2}^{N/2} e^{2ik_0(R_{\mathbf{z}}^n - R_{\mathbf{y}}^n)}$$

and

$$(2.21) \quad W_{\text{R}}(\mathbf{y}, \mathbf{z}) = \int_{\chi} \overline{A(t - 2R_{\mathbf{y}}^0/c)} A(t - 2R_{\mathbf{z}}^0/c) dt.$$

In (2.20),  $k_0 = \omega_0/c$  is the carrier wavenumber. In (2.21), we have (in accordance with (2.18))

$$R_{\mathbf{y}}^0 = |\mathbf{y} - \mathbf{x}^0| \quad \text{and} \quad R_{\mathbf{z}}^0 = |\mathbf{z} - \mathbf{x}^0|.$$

In [15, Appendix A], we have shown that the factorization error in (2.19) is small, on the order of the relative bandwidth, i.e., about  $B/\omega_0$ .

Hereafter, we will be using the Cartesian coordinates labeled by subscripts as follows: “1” will correspond to the azimuthal, or along-the-track, coordinate; “2” will correspond to the range coordinate, i.e., the horizontal coordinate normal to the track; and “3” will correspond to the vertical coordinate. With no loss of generality, we place the origin of the coordinate system within the beam footprint on the ground. In addition, we denote by  $\theta$  the angle of incidence, which is also referred to as the look angle. Then, the orbit altitude  $H = R \cos \theta$  and the distance from the origin to the ground track  $L = R \sin \theta$ ; see Figure 1.

An inspection of (2.19)–(2.21) shows that the GAF (2.17) is a function of only two independent spatial coordinates—the azimuthal direction, which corresponds to the variation of

$n$ , and the slant range direction, which is normal to the flight track and corresponds to the variation of  $R_{\mathbf{y}}$  and  $R_z$ . Hence, the SAR data collection algorithm that we have described (a monostatic noninterferometric sensor traveling along a linear trajectory) can generate only two-dimensional datasets (see also [6]). This results in a certain vagueness, because  $\nu(\mathbf{z})$  is a function of three variables and the integration in (2.16) is performed over a three-dimensional region ( $\mathbf{z} \in \mathbb{R}^3$ ). A standard way of removing this vagueness in the SAR ambiguity theory [5, 6, 8] consists of artificially restricting the dimension of the set on which  $\nu(\mathbf{z})$  is given. This is done by eliminating the vertical coordinate and defining the plane  $z_3 = 0$ , i.e., the surface of the Earth, as the locus of all the targets. Accordingly, the reflectivity function (2.12') becomes

$$(2.22) \quad \nu(\mathbf{z}) \equiv \nu(z_1, z_2, z_3) = \nu(z_1, z_2)\delta(z_3),$$

which is a single layer, or layer of monopoles, on the surface. From the standpoint of physics, considering the reflectivity in the form of (2.22) merely suggests that all the scattering occurs only at the surface of the target, which is what one intuitively expects when imaging the Earth from an aircraft or a satellite. The integration in (2.16) is then performed over a two-dimensional region (plane), and the resulting image reconstructs  $\nu(z_1, z_2)$ , i.e., yields the reflectivity on the surface of the Earth as a function of the two horizontal coordinates.

The individual factors  $W_{\Sigma}(\mathbf{y}, \mathbf{z})$  of (2.20) and  $W_R(\mathbf{y}, \mathbf{z})$  of (2.21) are computed in Appendix A; see also [15]. Specifically, the linearization of the travel distances yields (see (A.3))

$$(2.23) \quad R_z^n - R_{\mathbf{y}}^n \approx -\frac{Ll}{R} + \frac{(y_1 - z_1)x_1^n}{R},$$

where

$$x_1^n = \frac{nL_{SA}}{N} \quad \text{and} \quad l = y_2 - z_2.$$

For the length of the synthetic aperture, we assume  $L_{SA} \ll R$ . We also introduce

$$\Phi_0 = -2k_0 \frac{Ll}{R}.$$

Then, we perform the summation in (2.20) and get (see (A.5))

$$(2.24a) \quad W_{\Sigma}(\mathbf{y}, \mathbf{z}) \approx e^{i\Phi_0} W_A(\mathbf{y}, \mathbf{z}),$$

where

$$(2.24b) \quad W_A(\mathbf{y}, \mathbf{z}) = N \operatorname{sinc} \left( \pi \frac{y_1 - z_1}{\Delta_A} \right) \quad \text{and} \quad \Delta_A = \frac{\pi Rc}{\omega_0 L_{SA}}.$$

The quantity  $\Delta_A$  in formula (2.24b) is the azimuthal resolution. Altogether, the function  $W_A(\mathbf{y}, \mathbf{z})$  describes the performance of the SAR sensor in the azimuthal direction.

To calculate  $W_R$ , we perform the integration w.r.t.  $t$  in (2.21) and obtain (see (A.2))

$$(2.25) \quad W_R(\mathbf{y}, \mathbf{z}) \approx \tau \operatorname{sinc} \left( \pi \frac{R_{\mathbf{y}}^0 - R_z^0}{\Delta_R} \right), \quad \text{where} \quad \Delta_R = \frac{\pi c}{B}.$$

The quantity  $\Delta_R$  in (2.25) is the range resolution. The function  $W_R(\mathbf{y}, \mathbf{z})$  describes the performance of the SAR sensor in the range direction.

The overall expression for the GAF  $W(\mathbf{y}, \mathbf{z})$  of (2.17) becomes

$$(2.26) \quad W(\mathbf{y}, \mathbf{z}) = W_\Sigma(\mathbf{y}, \mathbf{z})W_R(\mathbf{y}, \mathbf{z}) = e^{i\Phi_0}W_A(\mathbf{y}, \mathbf{z})W_R(\mathbf{y}, \mathbf{z}).$$

We notice that, according to (2.23), (2.24), and (2.25), the GAF depends only on the difference of its arguments:  $W(\mathbf{y}, \mathbf{z}) = W(\mathbf{y} - \mathbf{z})$ , which indeed allows us to interpret (2.16) as a convolution integral. Each of the two factors,  $W_A$  and  $W_R$ , describes the spreading of the GAF in the corresponding direction, i.e., a measure of how different it is from the ideal  $\delta$ -function. We therefore see that the shape of the GAF  $W(\mathbf{y}, \mathbf{z})$  directly affects the quality of the reconstruction of  $\nu(\mathbf{z})$  in the form of  $I(\mathbf{y})$ ; see (2.16).

**2.2. Deficiencies of the conventional approach.** Earlier publications in the literature discussing the SAR ambiguity theory, including some of our own papers [29, 26, 14], did not distinguish between  $W_\Sigma(\mathbf{y}, \mathbf{z})$  and  $W_A(\mathbf{y}, \mathbf{z})$ , whereas these two factors are related by the fast phase multiplier  $e^{i\Phi_0}$ ; see (2.24a). As the absolute value of this multiplier is one, ignoring it has no effect on the expressions for resolution in either direction. That is why in the case of a point scatterer one can obtain the correct expressions for both range and azimuthal resolution even with the fast phase ignored [5, 8, 14, 26, 29]. For the case of extended scatterers, however, the fast phase in (2.16) should be retained.

The fast phase term  $e^{i\Phi_0}$  in (2.26) allows one to separate the scales of variation in both the imaged quantity  $\nu$  and the image  $I$  into fast (on the order of wavelength) and slow (much longer than the wavelength, on the order of resolution); see section 4. This, in turn, enables backscattering via the resonant Bragg mechanism and yields a physical interpretation of the observable quantity in SAR imaging as a slowly varying amplitude of the Bragg harmonic in the spectrum of ground reflectivity. Otherwise, consider, for example,  $n(\mathbf{z}) = \text{const}$  on a semispace. The reflection from such a target is specular and involves no backscattering. Yet if the reflectivity  $\nu(\mathbf{z})$  given by (2.12') for  $n(\mathbf{z}) = \text{const}$  is substituted into (2.16), and the fast phase term  $e^{i\Phi_0}$  is not included in  $W(\mathbf{y}, \mathbf{z})$ , then there will be a nonzero image intensity. This leads to an inconsistency, because (2.16) describes monostatic SAR imaging and therefore can generate an image only if a certain part of the incident field is scattered back to the antenna.

Moreover, the intensity of the image (2.16) for a homogeneous half-space will not depend on polarization, because the entire previous development is done in the scalar framework. In reality, however, the polarization needs to be taken into account. For a homogeneous target this was done in our recent work [13]. A more comprehensive inhomogeneous model introduced in section 3 will be generalized to the vector case in a forthcoming publication.

Another inconsistency in the traditional exposition of SAR ambiguity theory is related to the representation of the ground reflectivity function in the form of a single layer on the surface of the target; see (2.22). Such a representation is usually justified by the rapid decay of the radar signal as it penetrates below the Earth's surface (see, e.g., [5]). From the standpoint of physics, this is an adequate consideration because the typical SAR carrier frequencies are in the microwave range and their penetration depth is small.<sup>5</sup> It suggests, however, that the

---

<sup>5</sup>The penetration depth can often be estimated as one half of the wavelength.

scattering is strong, as it prevents the incident field from penetrating deep into the target. Hence, the condition for applicability of the first Born approximation, which assumes weak scattering, is violated. Moreover, a singular expression for  $\nu$  in (2.22) is an obvious violation of (2.5). The issue of equivalently representing a weakly scattering half-space by means of a single layer at the interface has been addressed in [13], but only for specular reflection.

In what follows, we address these concerns by introducing a new approach to the treatment of radar targets that will allow us to compute the scattered signal in any given direction. The new approach is more comprehensive than the previous one, as it carries no constraint that the scattering has to be weak and does not rely on the first Born approximation. Yet it keeps the inverse scattering problem for SAR linear and eventually allows one to obtain its solution in the form of convolution (2.16), where the integral is taken only along the surface of the target. When the scattering is weak, the results obtained in the new framework become equivalent to those obtained by means of the conventional approach.

**3. A half-space model for radar targets.** In this section, we modify the scattering model of section 2.1 in order to alleviate the difficulties outlined in section 2.2. Instead of a single layer on the surface, we consider a continuous scatterer in the form of a horizontally inhomogeneous dielectric half-space.<sup>6</sup> Allowing for inhomogeneity of the dielectric medium in the two horizontal directions and not in the vertical direction eventually lets us write the scattered field as a two-dimensional surface integral. This can be interpreted as scattering off the surface of the target only, in accordance with the aforementioned physical observation. Moreover, the half-space model enables linearization of either weak or strong scattering that is free of inconsistencies caused by choosing singular ground reflectivity functions.

To actually obtain the scattered field, we solve the governing wave equation by means of the separation of variables. In doing so, we first use the method of perturbations. Namely, we consider the dielectric permittivity as

$$\varepsilon(\mathbf{z}) = \varepsilon^{(0)}(\mathbf{z}) + \varepsilon^{(1)}(\mathbf{z}),$$

where  $\varepsilon^{(0)}(\mathbf{z})$  is a step function in the vertical direction equal to 1 in the upper half-space ( $z_3 > 0$ ) and a constant  $\varepsilon^{(0)}$  in the lower half-space ( $z_3 < 0$ ), and  $\varepsilon^{(1)}(\mathbf{z})$  is a perturbation, such that  $\varepsilon^{(1)}(\mathbf{z}) = 0$  for  $z_3 > 0$  and  $|\varepsilon^{(1)}(\mathbf{z})| \ll \varepsilon^{(0)}$ . Then, we seek the field in the form

$$u(t, \mathbf{z}) = u^{(0)}(t, \mathbf{z}) + u^{(1)}(t, \mathbf{z}),$$

where  $|u^{(1)}| \ll |u^{(0)}|$ , and linearize the scattering problem by dropping the higher order terms  $\sim \varepsilon^{(1)}u^{(1)}$ . Unlike in section 2.1, we do not require  $\varepsilon^{(0)} = 1$ , so that the scattering is not necessarily weak. When solving the linearized scattering problem by separation of variables, we employ two different approximations. We represent the incident field near the target as a plane wave, and we use the method of stationary phase to evaluate the inverse Fourier transform that yields the solution for the scattered field.

**3.1. Incident field near the target.** At every given moment of time, the radar antenna illuminates a region of size  $\sim L_{SA}$  on the ground; see Figure 2. As  $L_{SA} \ll R$ , within this small

---

<sup>6</sup>It is a generalization of the setup of [13], where the scatterer was a homogeneous (yet anisotropic) half-space.

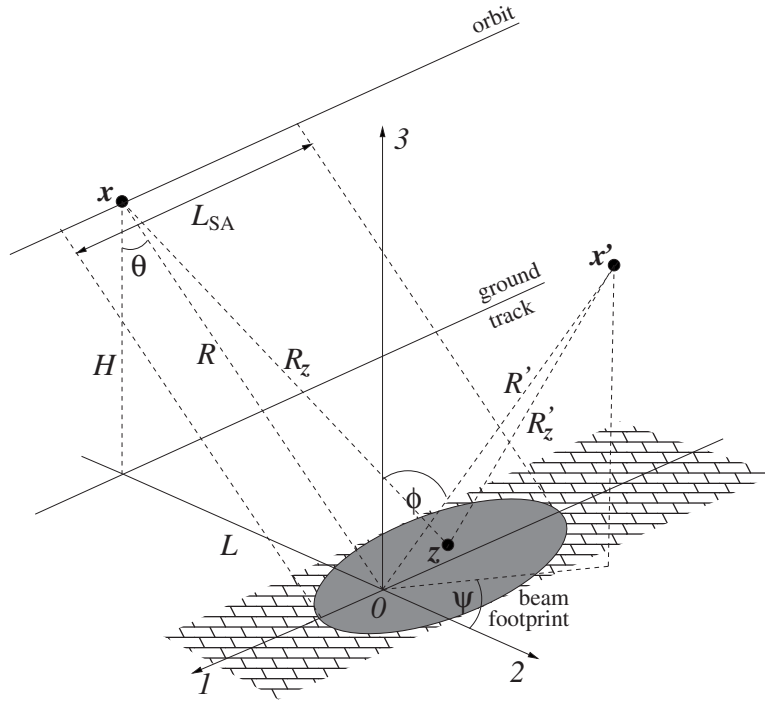


**Figure 2.** Schematic for the scattering geometry;  $\phi$  is the reflection angle, and  $\psi$  is the angle of deflection off the incidence plane (in this plot,  $\psi < 0$ ).

region (beam footprint) we can approximate the incident field by a plane wave, even though in reality it is a spherical wave confined to a narrow beam. For a single pulse emitted from  $\mathbf{x}^0$  toward the ground in the direction normal to the orbit, the plane wave approximation of the incident field (2.2) near the origin  $\mathbf{z} = (0, 0, 0)$  yields

$$(3.1) \quad u_i^{(0)}(t, \mathbf{z}) \approx \frac{1}{4\pi R} P \left( t - \frac{R}{c} - \frac{z_2}{c} \sin \theta + \frac{z_3}{c} \cos \theta \right),$$

where in the argument of  $P(\cdot)$  we have neglected the terms that are at least  $\sim z_2/R$  or  $\sim z_3/R$  times smaller than the retained terms, and in the denominator we have replaced the travel distance by the constant  $R$ , which is equivalent to disregarding the small amplitude variations of the incident field.

For the pulse  $P(t)$  given by (2.8), (2.9), we introduce its Fourier transform in time,

$$(3.2) \quad \tilde{P}(\omega) = \int_{-\infty}^{\infty} P(t) e^{i\omega t} dt = \int_{-\tau/2}^{\tau/2} P(t) e^{i\omega t} dt,$$

and rewrite (3.1) as

$$(3.3) \quad \begin{aligned} u_i^{(0)}(t, \mathbf{z}) &= \frac{1}{2\pi} \int_{-\infty}^{\infty} \tilde{u}_i^{(0)}(\omega, \mathbf{z}) e^{-i\omega t} d\omega \\ &\approx \frac{1}{2\pi} \frac{1}{4\pi R} \int_{-\infty}^{\infty} \tilde{P}(\omega) e^{i\frac{\omega}{c}(R+z_2 \sin \theta - z_3 \cos \theta)} e^{-i\omega t} d\omega, \end{aligned}$$

where  $\tilde{u}_i^{(0)}$  is the Fourier transform of  $u_i^{(0)}$ . Hereafter, the tilde above a character will denote the Fourier transform in time.

**3.2. The method of perturbations and the separation of variables.** Let the upper half-space of  $\mathbb{R}^3$  be occupied with a vacuum, and the lower half-space with a horizontally inhomogeneous dielectric material, such that the overall refractive index is

$$(3.4) \quad n^2(\mathbf{z}) = \varepsilon(\mathbf{z}) = \begin{cases} 1, & z_3 > 0, \\ \varepsilon^{(0)} + \varepsilon^{(1)}(z_1, z_2), & z_3 < 0. \end{cases}$$

In (3.4), we are additionally assuming that  $\varepsilon^{(1)}$  is a perturbation:  $|\varepsilon^{(1)}| \ll \varepsilon^{(0)} = \text{const}$ . We also emphasize that in (3.4) there is no variation of the refractive index with respect to the vertical coordinate  $z_3$ , except for the jump it undergoes at the horizontal plane  $z_3 = 0$ .

In the method of perturbations, we denote by  $u^{(0)}$  the zero order field, i.e., the field due to the constant part  $\varepsilon^{(0)}$  of  $n^2(\mathbf{z})$ . It is obtained by formally setting  $\varepsilon^{(1)} = 0$  in formula (3.4). As, however, the scattering is not necessarily weak ( $\varepsilon^{(0)}$  may be considerably greater than 1), the field  $u^{(0)}$  may not coincide with  $u_i^{(0)}$ . Then, we use the following representation:

$$(3.5) \quad u^{(0)} = \begin{cases} u_i^{(0)} + u_r^{(0)}, & z_3 > 0, \\ u_t^{(0)}, & z_3 < 0, \end{cases}$$

where  $u_r^{(0)}$  and  $u_t^{(0)}$  are the zero order reflected and transmitted fields, respectively.

To separate the variables in (2.3), we first Fourier transform it in time and for each  $\omega$  obtain a Helmholtz-type equation. Then, we extract the zero order terms and get<sup>7</sup>

$$(3.6) \quad \begin{aligned} (\Delta + k^2)(\tilde{u}_i^{(0)} + \tilde{u}_r^{(0)}) &= 0, & z_3 > 0, \\ (\Delta + \varepsilon^{(0)}k^2)\tilde{u}_t^{(0)} &= 0, & z_3 < 0, \end{aligned}$$

where  $k = \omega/c$ . For the first order, the method of perturbations yields

$$(3.7) \quad \begin{aligned} (\Delta + k^2)\tilde{u}^{(1)} &= 0, & z_3 > 0, \\ (\Delta + \varepsilon^{(0)}k^2)\tilde{u}^{(1)} &= -k^2\varepsilon^{(1)}\tilde{u}_t^{(0)}, & z_3 < 0, \end{aligned}$$

where on the right-hand side of the second equation (3.7) we keep only first order terms and neglect the terms of order two or higher. This is actually a linearization, which is equivalent to the first Born approximation in the case  $\varepsilon^{(0)} = 1$ .

Equations (3.6), (3.7) need to be supplemented by the interface conditions at  $z_3 = 0$ . We take those as the continuity of the total field and its normal derivative:<sup>8</sup>

$$(3.8) \quad \begin{aligned} (\tilde{u}^{(0)} + \tilde{u}^{(1)})|_{z_3=+0} &= (\tilde{u}^{(0)} + \tilde{u}^{(1)})|_{z_3=-0}, \\ \left( \frac{\partial \tilde{u}^{(0)}}{\partial z_3} + \frac{\partial \tilde{u}^{(1)}}{\partial z_3} \right) \Big|_{z_3=+0} &= \left( \frac{\partial \tilde{u}^{(0)}}{\partial z_3} + \frac{\partial \tilde{u}^{(1)}}{\partial z_3} \right) \Big|_{z_3=-0}. \end{aligned}$$

<sup>7</sup>The source term  $f$  is omitted because we are taking the incident field as a plane wave; see (3.1).

<sup>8</sup>In fact, it corresponds to the horizontal polarization of the incident and reflected electric field, with the reflected wave vector being in the incidence plane.

Equations (3.6), (3.7) also require radiation conditions as  $z_3 \rightarrow \pm\infty$ . Those will be specified for the transformed quantities after the separation of variables in space; see (3.16), (3.17), (3.18).

We first solve for zero order fields. From (3.3), we observe that

$$(3.9) \quad \tilde{u}_i^{(0)}(\omega, \mathbf{z}) = \mathbf{u}_i^{(0)} e^{ik(z_2 \sin \theta - z_3 \cos \theta)}, \quad \text{where} \quad \mathbf{u}_i^{(0)} = \frac{\tilde{P}(\omega) e^{ikR}}{4\pi R},$$

and for each  $\omega$  consider a transmission-reflection problem for the incident plane wave (3.9). The normal component of the wavenumber for the transmitted wave should have the same sign as that of the incident wave, whereas for the reflected wave the sign should be the opposite. Hence, we have

$$(3.10a) \quad \tilde{u}_r^{(0)} = \mathbf{u}_r^{(0)} e^{ik(z_2 \sin \theta + z_3 \cos \theta)},$$

$$(3.10b) \quad \tilde{u}_t^{(0)} = \mathbf{u}_t^{(0)} e^{i(kz_2 \sin \theta - k'z_3 \cos \theta')},$$

where  $\mathbf{u}_r^{(0)}$  and  $\mathbf{u}_t^{(0)}$  are the reflected and transmitted amplitudes, respectively;  $k' = k\sqrt{\varepsilon^{(0)}}$ ; and  $\theta'$  is the refraction angle determined from the second equation of (3.6):

$$\cos^2 \theta' = (\varepsilon^{(0)} k^2 - k^2 \sin^2 \theta) / k'^2 = 1 - \sin^2 \theta / \varepsilon^{(0)}.$$

In the method of perturbations, the continuity of the total field and its normal derivative at  $z_3 = 0$  (see (3.8)) translates into the separate continuity requirements for the zero order field and its normal derivative and for the first order field and its normal derivative. Continuity of  $\tilde{u}^{(0)}$  and  $\frac{\partial \tilde{u}^{(0)}}{\partial z_3}$  at  $z_3 = 0$  yields

$$(3.11) \quad \begin{aligned} \mathbf{u}_i^{(0)} + \mathbf{u}_r^{(0)} &= \mathbf{u}_t^{(0)}, \\ -ik \cos \theta \mathbf{u}_i^{(0)} + ik \cos \theta \mathbf{u}_r^{(0)} &= -ik' \cos \theta' \mathbf{u}_t^{(0)}. \end{aligned}$$

Equations (3.11) yield

$$(3.12) \quad \frac{\mathbf{u}_r^{(0)}}{\mathbf{u}_i^{(0)}} = -\frac{\sqrt{\varepsilon^{(0)}} \cos \theta' - \cos \theta}{\sqrt{\varepsilon^{(0)}} \cos \theta' + \cos \theta} \quad \text{and} \quad \frac{\mathbf{u}_t^{(0)}}{\mathbf{u}_i^{(0)}} = \frac{2 \cos \theta}{\sqrt{\varepsilon^{(0)}} \cos \theta' + \cos \theta}.$$

The right-hand sides of (3.12) are the well-known Fresnel reflection and transmission coefficients for the case of a horizontal polarization (the electric field is parallel to the surface).

To separate the variables in (3.7), we represent the perturbation of the dielectric coefficient  $\varepsilon^{(1)}$  and the first order field  $\tilde{u}^{(1)}$  as inverse Fourier transforms:

$$(3.13a) \quad \varepsilon^{(1)}(z_1, z_2) = \frac{1}{(2\pi)^2} \iint \hat{\varepsilon}^{(1)}(\zeta_1, \zeta_2) e^{i(\zeta_1 z_1 + \zeta_2 z_2)} d\zeta_1 d\zeta_2,$$

$$(3.13b) \quad \tilde{u}^{(1)}(\omega, z_1, z_2, z_3) = \frac{1}{(2\pi)^2} \iint \hat{u}^{(1)}(\omega, \zeta_1, \zeta_2, z_3) e^{i(\zeta_1 z_1 + \zeta_2 z_2)} d\zeta_1 d\zeta_2.$$

For convenience of notation, we have chosen opposite signs in the exponents for the transforms in space (3.13) and in time (3.3).<sup>9</sup>

<sup>9</sup>We would like the traveling plane waves to be represented as  $\sim e^{i(\mathbf{kz} - \omega t)}$ , where  $\mathbf{k} = (k_1, k_2, k_3)$ .

Substituting expressions (3.13), (3.10b) into (3.7) and taking the direct Fourier transform in space, we obtain the following uncoupled ordinary differential equations for each  $(\zeta_1, \zeta_2)$ :

$$(3.14) \quad \begin{cases} \left( \frac{d^2}{dz_3^2} + q^2 \right) \hat{u}^{(1)} = 0, & z_3 > 0, \\ \left( \frac{d^2}{dz_3^2} + q'^2 \right) \hat{u}^{(1)} = -k^2 \mathbf{u}_t^{(0)} \hat{\varepsilon}_\theta e^{-iq'_t z_3}, & z_3 < 0, \end{cases}$$

where

$$(3.15) \quad \begin{aligned} q^2 &= k^2 - \zeta_1^2 - \zeta_2^2, & q'^2 &= k'^2 - \zeta_1^2 - \zeta_2^2, \\ \hat{\varepsilon}_\theta &= \hat{\varepsilon}^{(1)}(\zeta_1, \zeta_2 - k \sin \theta), & \text{and } q'_t &= k' \cos \theta' = (k'^2 - k^2 \sin^2 \theta)^{1/2}. \end{aligned}$$

It is to be noted that the plane wave representation (3.10b) of the zero order transmitted field is valid as long as the plane wave representation (3.9) for the incident field is valid. The latter, in turn, is good within the antenna footprint on the ground, which is small compared to the distance from the antenna to the target (section 3.1). We therefore see that the right-hand side of the second equation (3.7) is compactly supported with respect to the variables  $(z_1, z_2)$  because of the factor  $\tilde{u}_t^{(0)}$ , which is a plane wave inside a narrow beam and zero elsewhere. However, when Fourier transforming this right-hand side in  $(z_1, z_2)$ , we obtain the frequency shift  $-k \sin \theta$  in the second argument of  $\hat{\varepsilon}^{(1)}$  (see (3.15)), as if the plane wave representation for  $\tilde{u}_t^{(0)}$  could be used everywhere. This apparent inconsistency is easy to resolve. Instead of attributing the compact support on the right-hand side of (3.7) to  $\tilde{u}_t^{(0)}$ , we can formally attribute it to the other factor,  $\varepsilon^{(1)} = \varepsilon^{(1)}(z_1, z_2)$ . Indeed, at every given moment of time the antenna illuminates only a small region of size  $\sim L_{\text{SA}} \ll R$  on the ground (the same beam footprint; see Figure 2), and no scattering occurs off of any other part of the plane  $z_3 = 0$ . Hence, instead of the true  $\varepsilon^{(1)}(z_1, z_2)$  we can consider its compactly supported restriction onto the beam footprint. On the one hand, this is not a limitation, because the size of this footprint is still much larger than the typical resolution [14]. On the other hand, having  $\varepsilon^{(1)}(z_1, z_2)$  compactly supported makes its Fourier transform  $\hat{\varepsilon}^{(1)}$  (see (3.13a)) infinitely smooth, which proves useful for the application of the method of stationary phase; see section 3.3.

A solution to system (3.14) will be sought as the sum of a general solution to the homogeneous system and a particular solution to the inhomogeneous system. The general solution is taken in the form

$$(3.16) \quad \hat{u}_g^{(1)} = \begin{cases} \mathbf{u}_i^{(0)} \mathbf{b} e^{iqz_3}, & z_3 > 0, \\ \mathbf{u}_i^{(0)} \mathbf{c} e^{-iq'z_3}, & z_3 < 0. \end{cases}$$

If the quantities  $q^2$  and  $q'^2$  introduced in (3.15) are positive,  $q^2 > 0$  and  $q'^2 > 0$ , then in the exponents in (3.16) we use the arithmetic roots,  $q = \sqrt{q^2} > 0$  and  $q' = \sqrt{q'^2} > 0$ . In that case, the general solution (3.16) is composed of two outgoing traveling waves: a wave traveling upward in the upper half-space ( $z_3 > 0$ ) and a wave traveling downward in the lower half-space ( $z_3 < 0$ ). Otherwise, if  $q^2 < 0$  or  $q'^2 < 0$ , then we define  $q = i\sqrt{|q^2|}$  or  $q' = i\sqrt{|q'^2|}$ , respectively, and the corresponding waves become evanescent. They decay exponentially away

from the interface  $z_3 = 0$ . This form of the general solution (given by (3.16) along with the foregoing choice of signs for  $q$  and  $q'$ ) is equivalent to enforcing the radiation of waves from the scattering surface  $z_3 = 0$  toward infinity. Indeed, in the first order field we have no incoming traveling waves and no evanescent waves that grow as  $|z_3| \rightarrow \infty$  either. Alternatively, we can say that the general solution  $\hat{u}_g^{(1)}$  of (3.16) satisfies the radiation conditions:

$$(3.17) \quad \begin{aligned} \frac{d\hat{u}_g^{(1)}}{dz_3} - iq\hat{u}_g^{(1)} &= 0 \quad \text{as } z_3 \rightarrow +\infty, \\ \frac{d\hat{u}_g^{(1)}}{dz_3} + iq'\hat{u}_g^{(1)} &= 0 \quad \text{as } z_3 \rightarrow -\infty. \end{aligned}$$

A particular solution needs to be built only inside the scattering material ( $z_3 < 0$ ), i.e., for the second equation of (3.14), which is inhomogeneous. Its form will depend on whether we are dealing with the resonant case  $q'^2 = q_r'^2$  or nonresonant case  $q'^2 \neq q_r'^2$ :

$$(3.18) \quad \hat{u}_p^{(1)} = \begin{cases} \mathbf{u}_i^{(0)} \mathbf{a}_1 e^{-iq'_r z_3} & \text{if } q'^2 \neq q_r'^2, \\ \mathbf{u}_i^{(0)} \mathbf{a}_2 z_3 e^{-iq'_r z_3} & \text{if } q'^2 = q_r'^2. \end{cases}$$

Note that the sign in the exponents in (3.18) also corresponds to the radiation of waves as  $z_3 \rightarrow -\infty$ . Substituting the first formula (3.18) into the second equation of (3.14), we get

$$(3.19) \quad \mathbf{a}_1 = \frac{k^2 \hat{\varepsilon}_\theta}{q_r'^2 - q'^2} \frac{\mathbf{u}_t^{(0)}}{\mathbf{u}_i^{(0)}} = \frac{k^2 \hat{\varepsilon}_\theta}{q_r'^2 - q'^2} \frac{2k \cos \theta}{q'_r + k \cos \theta} = \frac{k^2 \hat{\varepsilon}_\theta}{q_r'^2 - q'^2} \frac{2q_i}{q'_r + q_i},$$

where we have introduced another shorthand notation:

$$q_i = k \cos \theta.$$

Substituting the second formula (3.18) into the second equation of (3.14) for  $q' = q'_r$ , we have

$$(3.20) \quad \mathbf{a}_2 = \frac{k^2 \hat{\varepsilon}_\theta}{2iq'_r} \frac{\mathbf{u}_t^{(0)}}{\mathbf{u}_i^{(0)}} = \frac{k^2 \hat{\varepsilon}_\theta}{2iq'_r} \frac{2q_i}{q'_r + q_i}.$$

Note that the resonance may occur only for traveling waves, because  $q'_r > 0$ . The overall first order field is obtained by adding the general solution (3.16) and a particular solution (3.18):

$$(3.21) \quad \hat{u}^{(1)} = \hat{u}_g^{(1)} + \hat{u}_p^{(1)} = \begin{cases} \mathbf{u}_i^{(0)} \mathbf{b} e^{iqz_3}, & z_3 > 0, \\ \mathbf{u}_i^{(0)} \mathbf{c} e^{-iq'z_3} + \mathbf{u}_i^{(0)} \mathbf{a}_1 e^{-iq'_r z_3}, & z_3 < 0 \quad \text{and} \quad q'^2 \neq q_r'^2, \\ \mathbf{u}_i^{(0)} \mathbf{c} e^{-iq'z_3} + \mathbf{u}_i^{(0)} \mathbf{a}_2 z_3 e^{-iq'_r z_3}, & z_3 < 0 \quad \text{and} \quad q'^2 = q_r'^2, \end{cases}$$

where the coefficient  $\mathbf{a}_1$  is given by (3.19) and the coefficient  $\mathbf{a}_2$  is given by (3.20). The coefficients  $\mathbf{b}$  and  $\mathbf{c}$  in (3.21) need to be determined from the interface conditions, which require the continuity of  $\hat{u}^{(1)}$  and  $\frac{d\hat{u}^{(1)}}{dz_3}$  at  $z_3 = 0$ . In the nonresonant case we have

$$\begin{aligned} \mathbf{b} &= \mathbf{c} + \mathbf{a}_1, \\ iq\mathbf{b} &= -iq'\mathbf{c} - iq'_r \mathbf{a}_1, \end{aligned}$$

which yields for  $z_3 > 0$  (see (3.19))

$$(3.22) \quad \begin{aligned} \mathbf{b} &= \mathbf{a}_1 \frac{q' - q'_r}{q' + q} = \frac{k^2 \hat{\varepsilon}_\theta}{q_r'^2 - q'^2} \frac{2q_i}{q'_r + q_i} \frac{q' - q'_r}{q' + q} \\ &= -2\hat{\varepsilon}_\theta \frac{k^2 q_i}{(q' + q)(q'_r + q')(q'_r + q_i)}. \end{aligned}$$

In the resonant case, the continuity of  $\hat{u}^{(1)}$  and  $\frac{d\hat{u}^{(1)}}{dz_3}$  at  $z_3 = 0$  implies

$$\begin{aligned} \mathbf{b} &= \mathbf{c}, \\ iq\mathbf{b} &= -iq'_r\mathbf{c} + \mathbf{a}_2, \end{aligned}$$

which for  $z_3 > 0$  results in (see (3.20))

$$(3.23) \quad \begin{aligned} \mathbf{b} &= \frac{\mathbf{a}_2}{i(q'_r + q)} = \frac{1}{i(q'_r + q)} \frac{k^2 \hat{\varepsilon}_\theta}{2iq'_r} \frac{2q_i}{q'_r + q_i} \\ &= -2\hat{\varepsilon}_\theta \frac{k^2 q_i}{(q'_r + q)2q'_r(q'_r + q_i)}. \end{aligned}$$

A very important observation that one can make right away is that the first order solution  $\hat{u}^{(1)}$  in a vacuum ( $z_3 > 0$ ) is insensitive to the resonances in the material. Indeed, if we substitute  $q' = q'_r$  into the expression (3.22) for the nonresonant coefficient  $\mathbf{b}$ , we obtain the expression (3.23) for the same coefficient  $\mathbf{b}$  in the resonant regime. This is convenient, as it allows us to use one and the same expression uniformly for the entire range of  $q$  and  $q'$  when bringing the solution for  $z_3 > 0$  back from the transformed space first to the frequency domain (see section 3.3) and then to the time domain (see section 3.4).

Note also that we have computed only the coefficients  $\mathbf{b}$  (see (3.22), (3.23)) and did not compute the coefficients  $\mathbf{c}$  for (3.21), because hereafter we will mostly be interested in analyzing the reflected field, i.e., the solution for  $z_3 > 0$ . We also observe that, regardless of the value of  $\mathbf{c}$ , the solution (3.21) in the resonant case  $q'^2 = q_r'^2$  is unbounded as  $z_3 \rightarrow -\infty$ . This behavior is obviously nonphysical. It has, however, been mentioned in the literature that if the scattering is weak, then the linearization based on the first Born approximation is ill-suited for describing the field inside the material; see, e.g., [21, 22].<sup>10</sup> Apparently, this deficiency of the first Born approximation has been inherited by our model, which does not assume that the scattering is weak yet employs the linearization. On the other hand, despite its suboptimal performance inside the material, the first Born approximation is known to work well for the scattered field in the vacuum region; see [21, 22]. Moreover, in our recent work [13] we have thoroughly analyzed the case of a specular reflection off a homogeneous material half-space and shown that the reflection coefficients obtained with the help of the first Born approximation coincide with the linearized true Fresnel coefficients, which correspond to the well-known exact scattering solution. In the current paper, this motivates the use of a similar

---

<sup>10</sup>The transmitted field is better described by the so-called Rytov approximation; see, e.g., [3, Chapter XIII]. On the other hand, the nonphysical unboundedness of the solution obtained by means of the first Born approximation in the material in the resonant case can be removed by adding a small dissipation, in the spirit of the limiting absorption principle.

yet more general linearization for describing the solution in vacuum for the field scattered off a more sophisticated target (inhomogeneous dielectric half-space), for which no exact solution is available. The linearized solution that we obtain in vacuum ( $z_3 > 0$ ) always remains bounded regardless of its behavior inside the material ( $z_3 < 0$ ).

**3.3. Reflected field in the frequency domain.** The first order reflected field at  $\mathbf{x}' \in \mathbb{R}^3$ ,  $x'_3 > 0$ , is the inverse Fourier transform (3.13b) of the solution  $\hat{u}^{(1)}$  given by the first line of (3.21),

$$\begin{aligned}\tilde{u}^{(1)}(\omega, \mathbf{x}') &= \frac{1}{(2\pi)^2} \iint \mathbf{u}_i^{(0)} \mathbf{b} e^{iqx'_3} e^{i(\zeta_1 x'_1 + \zeta_2 x'_2)} d\zeta_1 d\zeta_2 \\ &= \frac{k^2}{(2\pi)^2} \iint \mathbf{u}_i^{(0)} \mathbf{b} e^{i\sqrt{1-\eta_1^2-\eta_2^2}\xi_3} e^{i(\eta_1\xi_1+\eta_2\xi_2)} d\eta_1 d\eta_2,\end{aligned}$$

where we used the definition of  $q$  from (3.15) and made all the quantities in the exponents dimensionless for future convenience:

$$x'_j = \frac{1}{k}\xi_j, \quad j = 1, 2, 3, \quad \text{and} \quad \zeta_j = k\eta_j, \quad j = 1, 2.$$

The previous integral gets naturally split into two according to whether the square root in the first exponent is real or imaginary:

$$\begin{aligned}(3.24) \quad \tilde{u}^{(1)}(\omega, \mathbf{x}') &= \frac{\mathbf{u}_i^{(0)} k^2}{(2\pi)^2} \iint_{\eta_1^2 + \eta_2^2 < 1} \mathbf{b} e^{i\kappa\xi_3} d\eta_1 d\eta_2 \\ &+ \frac{\mathbf{u}_i^{(0)} k^2}{(2\pi)^2} \iint_{\eta_1^2 + \eta_2^2 > 1} \mathbf{b} e^{-\sqrt{\eta_1^2 + \eta_2^2 - 1}\xi_3} e^{i(\eta_1\xi_1 + \eta_2\xi_2)} d\eta_1 d\eta_2.\end{aligned}$$

In (3.24), we take  $\mathbf{b} = \mathbf{b}(\eta_1, \eta_2)$  from (3.22) with (cf. (3.15))

$$(3.25) \quad q^2 = k^2(1 - \eta_1^2 - \eta_2^2) \quad \text{and} \quad q'^2 = k^2(k'^2/k^2 - \eta_1^2 - \eta_2^2).$$

The phase function  $\kappa$  in the first integral of (3.24) is defined as

$$(3.26) \quad \kappa = \kappa(\eta_1, \eta_2, \xi_1, \xi_2, \xi_3) = \sqrt{1 - \eta_1^2 - \eta_2^2} + \frac{\xi_1}{\xi_3}\eta_1 + \frac{\xi_2}{\xi_3}\eta_2.$$

Note that the first integral on the right-hand side of (3.24) corresponds to traveling waves, and the second one to evanescent waves; see the discussion after (3.16). We need to evaluate (3.24) in the far field, i.e., far away from the small region on the surface of the Earth that returns the scattered waves (the beam footprint), which means  $\xi_3 \gg 1$ . The analysis will be similar yet not identical for the two cases:  $\varepsilon^{(0)} > 1$  and  $\varepsilon^{(0)} = 1$  (the latter case corresponds to weak scattering).

First, we will take  $\varepsilon^{(0)} > 1$  and estimate the contribution of evanescent waves to  $\tilde{u}^{(1)}(\omega, \mathbf{x}')$ , i.e., the second integral on the right-hand side of (3.24). In that regard, we notice that as  $k' = k\sqrt{\varepsilon^{(0)}} > 1$ , the function  $\mathbf{b} = \mathbf{b}(\eta_1, \eta_2)$  is smooth and bounded everywhere. Indeed, the fraction on the right-hand side of the last equality of (3.22) is smooth and bounded because  $q$  and  $q'$  may not turn into zero simultaneously (see (3.25)), and as we additionally have both

$q_i > 0$  and  $q'_i > 0$ , none of the three factors in the denominator may ever become equal to zero. Moreover,  $\hat{\varepsilon}_\theta = \hat{\varepsilon}^{(1)}(k\eta_1, k\eta_2 - k \sin \theta)$  is smooth and bounded since the first order permittivity  $\varepsilon^{(1)}(z_1, z_2)$  is considered compactly supported and hence its Fourier transform is smooth and bounded; see (3.13a). Consequently, we can write

$$(3.27) \quad \begin{aligned} & \left| \iint_{\eta_1^2 + \eta_2^2 > 1} \mathfrak{b} e^{-\sqrt{\eta_1^2 + \eta_2^2 - 1} \xi_3} e^{i(\eta_1 \xi_1 + \eta_2 \xi_2)} d\eta_1 d\eta_2 \right| \\ & \leq \text{const} \cdot \iint_{\eta_1^2 + \eta_2^2 > 1} e^{-\sqrt{\eta_1^2 + \eta_2^2 - 1} \xi_3} d\eta_1 d\eta_2 \\ & = \text{const} \cdot 2\pi \cdot \int_1^\infty e^{-\sqrt{\rho^2 - 1} \xi_3} \rho d\rho = \mathcal{O}(\xi_3^{-2}), \end{aligned}$$

which means that the contribution of evanescent waves to the first order scattered field decays no more slowly than the inverse square of the vertical distance from the scattering region.

The contribution of traveling waves to  $\tilde{u}^{(1)}(\omega, \mathbf{x}')$  for  $\varepsilon^{(0)} > 1$ , i.e., the first integral on the right-hand side of (3.24), can be evaluated using the method of stationary phase [9]. The large parameter for the method of stationary phase is  $\xi_3 \gg 1$ . To apply this method, we need to consider a fixed viewing direction defined by the reflection angle  $\phi$  and the angle  $\psi$  of deflection of the scattered signal from the incidence plane:

$$(3.28) \quad \frac{x'_1}{x'_3} = \frac{\xi_1}{\xi_3} = \tan \phi \sin \psi \quad \text{and} \quad \frac{x'_2}{x'_3} = \frac{\xi_2}{\xi_3} = \tan \phi \cos \psi.$$

The angles  $\phi$  and  $\psi$  are equivalent to the standard spherical angles; in particular, for the case of backscattering (monostatic imaging,  $\mathbf{x} = \mathbf{x}'$ ) we would have  $\phi = \theta$  and  $\psi = \pi$ , whereas for the case of specular reflection we would have  $\phi = \theta$  and  $\psi = 0$ ; see Figure 2.

A stationary point of the phase function (3.26) with respect to the variables  $(\eta_1, \eta_2)$  is a solution to the following system of two equations:

$$(3.29) \quad \begin{aligned} \frac{\partial \kappa}{\partial \eta_1} &= -\frac{\eta_1}{\sqrt{1 - \eta_1^2 - \eta_2^2}} + \frac{\xi_1}{\xi_3} = 0, \\ \frac{\partial \kappa}{\partial \eta_2} &= -\frac{\eta_2}{\sqrt{1 - \eta_1^2 - \eta_2^2}} + \frac{\xi_2}{\xi_3} = 0. \end{aligned}$$

Squaring each equation of (3.29) and solving, we obtain

$$\begin{aligned} \eta_{s,1}^2 &= \frac{\xi_1^2}{\xi_1^2 + \xi_2^2 + \xi_3^2} = \sin^2 \phi \sin^2 \psi, \\ \eta_{s,2}^2 &= \frac{\xi_2^2}{\xi_1^2 + \xi_2^2 + \xi_3^2} = \sin^2 \phi \cos^2 \psi. \end{aligned}$$

This system of equations has a total of four roots, but only one of those actually satisfies (3.29):

$$(3.30) \quad \begin{aligned} \eta_{s,1} &= \sin \phi \sin \psi, \\ \eta_{s,2} &= \sin \phi \cos \psi. \end{aligned}$$

Solution (3.30) yields a unique isolated stationary point of the phase function (3.26) within the domain  $\{\eta_1^2 + \eta_2^2 < 1\}$  of the first integral (3.24). Moreover, for the determinant of the Hessian matrix  $H(\kappa) = \{\partial^2 \kappa / \partial \eta_i \partial \eta_j\}$  of (3.26) we have

$$\det H(\kappa) = \begin{vmatrix} \frac{\partial^2 \kappa}{\partial \eta_1^2} & \frac{\partial^2 \kappa}{\partial \eta_1 \partial \eta_2} \\ \frac{\partial^2 \kappa}{\partial \eta_1 \partial \eta_2} & \frac{\partial^2 \kappa}{\partial \eta_2^2} \end{vmatrix} = \begin{vmatrix} -\frac{1-\eta_2^2}{(1-\eta_1^2-\eta_2^2)^{3/2}} & -\frac{\eta_1 \eta_2}{(1-\eta_1^2-\eta_2^2)^{3/2}} \\ -\frac{\eta_1 \eta_2}{(1-\eta_1^2-\eta_2^2)^{3/2}} & -\frac{1-\eta_1^2}{(1-\eta_1^2-\eta_2^2)^{3/2}} \end{vmatrix} = \frac{1}{(1-\eta_1^2-\eta_2^2)^2},$$

and consequently,  $\det H(\kappa(\eta_{s,1}, \eta_{s,2})) = \cos^{-4} \phi$ . Hence, the stationary point (3.30) is non-degenerate, provided that the reflection angle  $\phi$  is less than  $\pi/2$ . Therefore, we can directly apply the method of stationary phase [9] for approximating the first integral (3.24), as long as the propagation direction for the reflected wave is not parallel to the surface:<sup>11</sup>

$$(3.31) \quad \iint_{\eta_1^2 + \eta_2^2 < 1} \mathbf{b} e^{i\kappa \xi_3} d\eta_1 d\eta_2 = \frac{2\pi}{\xi_3} e^{i\kappa(\eta_{s,1}, \eta_{s,2})\xi_3} e^{i\pi/2} \left[ \frac{\mathbf{b}(\eta_{s,1}, \eta_{s,2})}{\sqrt{|\det H(\kappa(\eta_{s,1}, \eta_{s,2}))|}} + \mathcal{O}(\xi_3^{-1}) \right] \\ = \frac{2\pi i}{\xi_3} e^{i\xi_3 / \cos \phi} \mathbf{b}(\eta_{s,1}, \eta_{s,2}) \cos^2 \phi + \mathcal{O}(\xi_3^{-2}).$$

Comparing formulae (3.27) and (3.31), we conclude that for  $\varepsilon^{(0)} > 1$  the contribution of traveling waves dominates in the overall expression for  $\tilde{u}^{(1)}(\omega, \mathbf{x}')$  in the far field ( $\xi_3 \gg 1$ ). Thus, we will neglect all the terms  $\mathcal{O}(\xi_3^{-2})$  hereafter and use (3.9), (3.15), (3.22), and (3.24) to write the first order scattered field in the following form:

(3.32)

$$\tilde{u}^{(1)}(\omega, \mathbf{x}') \approx \frac{i\mathbf{u}_i^{(0)} \mathbf{b}(\eta_{s,1}, \eta_{s,2}) k \cos \phi e^{ikR'}}{2\pi R'} \\ = -\frac{i\tilde{P}(\omega)}{4\pi^2} k \hat{\varepsilon}^{(1)}(k \sin \phi \sin \psi, k \sin \phi \cos \psi - k \sin \theta) \mathcal{M}(\varepsilon^{(0)}, \theta, \phi) \frac{e^{ikR}}{R} \frac{e^{ikR'}}{R'},$$

where  $R' = \xi_3/k \cos \phi = (x_1'^2 + x_2'^2 + x_3'^2)^{1/2}$  (see Figure 2) and

(3.33)  $\mathcal{M}(\varepsilon^{(0)}, \theta, \phi)$

$$= \frac{\cos \theta \cos \phi}{(\cos \phi + \sqrt{\varepsilon^{(0)} - \sin^2 \phi})(\sqrt{\varepsilon^{(0)} - \sin^2 \phi} + \sqrt{\varepsilon^{(0)} - \sin^2 \theta})(\cos \theta + \sqrt{\varepsilon^{(0)} - \sin^2 \theta})}.$$

For monostatic imaging ( $\mathbf{x} = \mathbf{x}'$ ) we have  $\phi = \theta$  and  $\psi = \pi$ , so in (3.32) the arguments of  $\hat{\varepsilon}^{(1)}$  simplify and we get  $\hat{\varepsilon}^{(1)}(0, -2k \sin \theta)$ .

The case of  $\varepsilon^{(0)} = 1$ , which corresponds to weak scattering, requires special analysis, because the reflection coefficient  $\mathbf{b}$  of (3.22) may become singular. Indeed, in this case  $k' = k\sqrt{\varepsilon^{(0)}} = k$  and hence  $q' = q$ ; see (3.15). Therefore, the first factor in the denominator on the right-hand side of (3.22) may become zero.

<sup>11</sup>For small grazing angles, having a large vertical distance  $\xi_3$  implies an excessively large horizontal distance.

To evaluate the contribution of evanescent waves to  $\tilde{u}^{(1)}(\omega, \mathbf{x}')$ , i.e., the second integral on the right-hand side of (3.24), we first change the variables,  $\eta_1 = \rho \cos \varphi$ ,  $\eta_2 = \rho \sin \varphi$ , so that

$$(3.34) \quad \begin{aligned} & \iint_{\eta_1^2 + \eta_2^2 > 1} \mathfrak{b} e^{-\sqrt{\eta_1^2 + \eta_2^2 - 1} \xi_3} e^{i(\eta_1 \xi_1 + \eta_2 \xi_2)} d\eta_1 d\eta_2 \\ &= \int_1^\infty \frac{e^{-\sqrt{\rho^2 - 1} \xi_3}}{2\sqrt{\rho^2 - 1}} \int_0^{2\pi} \mathfrak{b}' e^{i(\rho \cos \varphi \xi_1 + \rho \sin \varphi \xi_2)} d\varphi \rho d\rho, \end{aligned}$$

where  $\mathfrak{b}'$  represents the nonsingular part of  $\mathfrak{b}$  of (3.22) for the case  $\varepsilon^{(0)} = 1$ :

$$\mathfrak{b}' \stackrel{\text{def}}{=} \frac{2q\mathfrak{b}}{k}.$$

For a given viewing direction (3.28), we will estimate the integral with respect to  $\varphi$  on the right-hand side of (3.34) by the method of stationary phase. Using (3.28), we can write

$$(3.35) \quad \begin{aligned} \rho \cos \varphi \xi_1 + \rho \sin \varphi \xi_2 &= \rho \sqrt{\xi_1^2 + \xi_2^2} \left( \frac{\xi_1}{\sqrt{\xi_1^2 + \xi_2^2}} \cos \varphi + \frac{\xi_2}{\sqrt{\xi_1^2 + \xi_2^2}} \sin \varphi \right) \\ &= \rho \xi_3 \tan \phi (\sin \psi \cos \varphi + \cos \psi \sin \varphi) = \xi_3 \rho \tan \phi \sin(\varphi + \psi). \end{aligned}$$

The phase function  $\rho \tan \phi \sin(\varphi + \psi)$  has two isolated nondegenerate stationary points (with respect to  $\varphi$ ) given by  $\cos(\varphi + \psi) = 0$ . At these points, clearly,  $|\sin(\varphi + \psi)| = 1$ , and therefore, for  $\xi_3 \gg 1$  the method of stationary phase yields

$$\left| \int_0^{2\pi} \mathfrak{b}' e^{i(\rho \cos \varphi \xi_1 + \rho \sin \varphi \xi_2)} d\varphi \right| \approx (\mathfrak{b}'_1 + \mathfrak{b}'_2) \sqrt{\frac{2\pi}{\xi_3 \rho \tan \phi}} (1 + \mathcal{O}(\xi_3^{-1})),$$

where  $\mathfrak{b}'_1$  and  $\mathfrak{b}'_2$  on the right-hand side are the values of  $\mathfrak{b}'$  at the stationary points (that still depend on  $\rho$ ). As  $\mathfrak{b}'$  is smooth and bounded everywhere, for  $\phi > 0$  and  $\rho > 1$  (as in (3.34)), we can write

$$\left| \int_0^{2\pi} \mathfrak{b}' e^{i(\rho \cos \varphi \xi_1 + \rho \sin \varphi \xi_2)} d\varphi \right| \leq \frac{\text{const}}{\sqrt{\xi_3}} (1 + \mathcal{O}(\xi_3^{-1})).$$

Therefore, for the overall integral (3.34) we have

$$(3.36) \quad \begin{aligned} & \left| \int_1^\infty \frac{e^{-\sqrt{\rho^2 - 1} \xi_3}}{2\sqrt{\rho^2 - 1}} \int_0^{2\pi} \mathfrak{b}' e^{i(\rho \cos \varphi \xi_1 + \rho \sin \varphi \xi_2)} d\varphi \rho d\rho \right| \\ & \leq \frac{\text{const}}{\sqrt{\xi_3}} (1 + \mathcal{O}(\xi_3^{-1})) \int_1^\infty \frac{e^{-\sqrt{\rho^2 - 1} \xi_3}}{2\sqrt{\rho^2 - 1}} \rho d\rho = \frac{\text{const}}{\xi_3^{3/2}} + \mathcal{O}(\xi_3^{-5/2}). \end{aligned}$$

Estimate (3.36) shows that the contribution of evanescent waves to the first order scattered field in the case  $\varepsilon^{(0)} = 1$  (weak scattering) decays at least as fast as the reciprocal vertical distance raised to the power three halves. This decay is slower (by half order) than the one we have obtained in the case  $\varepsilon^{(0)} > 1$ ; see (3.27).

For the first integral on the right-hand side of (3.24), where the phase function  $\kappa$  is given by (3.26), we employ the same change of variables as in (3.34) (see also (3.35)):

$$\begin{aligned}
(3.37) \quad & \iint_{\eta_1^2 + \eta_2^2 < 1} \mathbf{b} e^{i\kappa\xi_3} d\eta_1 d\eta_2 \\
&= \int_0^1 \int_0^{2\pi} \mathbf{b}' e^{i \left( \sqrt{1-\rho^2} \xi_3 + \rho \cos \varphi \xi_1 + \rho \sin \varphi \xi_2 \right)} \frac{d\varphi \rho d\rho}{2\sqrt{1-\rho^2}} \\
&= \frac{1}{2} \int_0^1 \int_0^{2\pi} \mathbf{b}' e^{i\xi_3 \left( \varrho + \tan \phi \sqrt{1-\varrho^2} \sin(\varphi + \psi) \right)} d\varphi d\varrho,
\end{aligned}$$

where  $1 - \rho^2 = \varrho^2$ . As  $\mathbf{b}'$  is smooth and bounded everywhere, for  $\xi_3 \gg 1$  the last integral of (3.37) can be approximated using the method of stationary phase. Consider the phase function  $\kappa$  as a function of the new variables (cf. (3.26)):

$$(3.38) \quad \kappa = \kappa(\varphi, \varrho, \phi, \psi) = \varrho + \tan \phi \sqrt{1 - \varrho^2} \sin(\varphi + \psi).$$

Its stationary points with respect to the variables  $(\varphi, \varrho)$  satisfy the following system:

$$\begin{aligned}
(3.39) \quad & \frac{\partial \kappa}{\partial \varphi} = \tan \phi \sqrt{1 - \varrho^2} \cos(\varphi + \psi) = 0, \\
& \frac{\partial \kappa}{\partial \varrho} = 1 - \frac{\varrho \tan \phi}{\sqrt{1 - \varrho^2}} \sin(\varphi + \psi) = 0.
\end{aligned}$$

The first equation of (3.39) implies that either  $\varrho_s = 1$  or  $\cos(\varphi_s + \psi) = 0$ . Yet  $\varrho_s = 1$  does not satisfy the second equation of (3.39), and hence for a stationary point  $(\varphi_s, \varrho_s)$  of (3.38) we must have  $\cos(\varphi_s + \psi) = 0$ . Consequently,  $\sin(\varphi_s + \psi) = 1$  or  $\sin(\varphi_s + \psi) = -1$ , but the second choice does not satisfy the second equation of (3.39). Then, for  $\sin(\varphi_s + \psi) = 1$  the second equation of (3.39) yields  $\varrho_s = \cos \phi$ , and we conclude that the phase function  $\kappa$  of (3.38) has a unique stationary point on the domain  $\{0 < \varphi < 2\pi, 0 < \varrho < 1\}$  of the last integral (3.37):

$$\begin{aligned}
(3.40) \quad & \cos(\varphi_s + \psi) = 0, \\
& \varrho_s = \cos \phi.
\end{aligned}$$

It is easy to see that the stationary point (3.40) of the phase function (3.38) is the same as the previously found stationary point (3.30) of the phase function (3.26) in the coordinates  $(\eta_1, \eta_2)$ . Indeed, the first equation of (3.40) implies that  $\cos \varphi_s = \sin \psi$  and  $\sin \varphi_s = \cos \psi$ , and then  $\eta_{s,1} = \sqrt{1 - \varrho_s^2} \cos \varphi_s = \sin \phi \sin \psi$  and  $\eta_{s,2} = \sqrt{1 - \varrho_s^2} \sin \varphi_s = \sin \phi \cos \psi$ .

The stationary point (3.40) is also nondegenerate. To see that, we write<sup>12</sup>

$$\underbrace{\begin{bmatrix} \frac{\partial^2 \kappa}{\partial \varphi^2} & \frac{\partial^2 \kappa}{\partial \varphi \partial \varrho} \\ \frac{\partial^2 \kappa}{\partial \varphi \partial \varrho} & \frac{\partial^2 \kappa}{\partial \varrho^2} \end{bmatrix}}_{H(\kappa(\varphi, \varrho))} = \underbrace{\begin{bmatrix} \frac{\partial \eta_1}{\partial \varphi} & \frac{\partial \eta_2}{\partial \varphi} \\ \frac{\partial \eta_1}{\partial \varrho} & \frac{\partial \eta_2}{\partial \varrho} \end{bmatrix}}_{J^T} \underbrace{\begin{bmatrix} \frac{\partial^2 \kappa}{\partial \eta_1^2} & \frac{\partial^2 \kappa}{\partial \eta_1 \partial \eta_2} \\ \frac{\partial^2 \kappa}{\partial \eta_1 \partial \eta_2} & \frac{\partial^2 \kappa}{\partial \eta_2^2} \end{bmatrix}}_{H(\kappa(\eta_1, \eta_2))} \underbrace{\begin{bmatrix} \frac{\partial \eta_1}{\partial \varphi} & \frac{\partial \eta_1}{\partial \varrho} \\ \frac{\partial \eta_2}{\partial \varphi} & \frac{\partial \eta_2}{\partial \varrho} \end{bmatrix}}_J,$$

<sup>12</sup>This relation holds only at stationary points.

where the Jacobi matrix is given by

$$J = \begin{bmatrix} -\sqrt{1-\varrho^2} \sin \varphi & -\frac{\varrho}{\sqrt{1-\varrho^2}} \cos \varphi \\ \sqrt{1-\varrho^2} \cos \varphi & -\frac{\varrho}{\sqrt{1-\varrho^2}} \sin \varphi \end{bmatrix},$$

so that  $\det J = \det J^T = \varrho$ , and at the stationary point (3.40) we have

$$\det H(\kappa(\varphi_s, \varrho_s)) = \varrho_s \det H(\kappa(\eta_{s,1}, \eta_{s,2})) \varrho_s = \cos \phi \cos^{-4} \phi \cos \phi = \cos^{-2} \phi.$$

Therefore, the last integral of (3.37) can be approximated as follows (cf. (3.31)):

$$\begin{aligned} & \frac{1}{2} \int_0^1 \int_0^{2\pi} \mathbf{b}' e^{i\xi_3 (\varrho + \tan \phi \sqrt{1-\varrho^2} \sin(\varphi+\psi))} d\varphi d\varrho \\ (3.41) \quad &= \frac{1}{2} \frac{2\pi}{\xi_3} e^{i\kappa(\varphi_s, \varrho_s) \xi_3} e^{i\pi/2} \left[ \frac{\mathbf{b}'(\varphi_s, \varrho_s)}{\sqrt{|\det H(\kappa(\varphi_s, \varrho_s))|}} + \mathcal{O}(\xi_3^{-1}) \right] \\ &= \frac{2\pi i}{\xi_3} e^{i\xi_3 / \cos \phi} \frac{\mathbf{b}'(\varphi_s, \varrho_s)}{2} \cos \phi + \mathcal{O}(\xi_3^{-2}). \end{aligned}$$

Comparing (3.36) and (3.41), we can determine that, similarly to the case  $\varepsilon^{(0)} > 1$ , the contribution of traveling waves in the far field ( $\xi_3 \gg 1$ ) dominates in the overall expression for  $\tilde{u}^{(1)}(\omega, \mathbf{x}')$  in the case  $\varepsilon^{(0)} = 1$  as well. Therefore, from now on we will disregard all the terms that decay faster than  $\mathcal{O}(\xi_3^{-1})$ , which yields (cf. (3.32))

$$\begin{aligned} (3.32') \quad \tilde{u}^{(1)}(\omega, \mathbf{x}') &\approx \frac{i u_1^{(0)}}{2\pi} \frac{\mathbf{b}'(\varphi_s, \varrho_s) k}{2} \frac{e^{ikR'}}{R'} \\ &= -\frac{i\tilde{P}(\omega)}{4\pi^2} k \varepsilon^{(1)} (k \sin \phi \sin \psi, k \sin \phi \cos \psi - k \sin \theta) \mathcal{M}'(\theta, \phi) \frac{e^{ikR}}{R} \frac{e^{ikR'}}{R'}, \end{aligned}$$

where

$$(3.33') \quad \mathcal{M}'(\theta, \phi) = \frac{1}{4(\cos \phi + \cos \theta)}.$$

We see that the function  $\mathcal{M}'(\theta, \phi)$  of (3.33') can be obtained by formally substituting  $\varepsilon^{(0)} = 1$  into the expression (3.33) for  $\mathcal{M}(\varepsilon^{(0)}, \theta, \phi)$ . Hence, the first order scattered field  $\tilde{u}^{(1)}(\omega, \mathbf{x}')$  given by (3.32') in the case  $\varepsilon^{(0)} = 1$  can also be obtained from the more general expression (3.32) that covers the case  $\varepsilon^{(0)} > 1$  by formally substituting  $\varepsilon^{(0)} = 1$ . We therefore conclude that there is no need to keep the separate expressions for  $\varepsilon^{(0)} > 1$  and  $\varepsilon^{(0)} = 1$ , and that formulae (3.32), (3.33) can be used for the entire range  $\varepsilon^{(0)} \geq 1$ .

An examination of (3.32) shows that for large propagation distances  $R'$  the first order scattered field  $\tilde{u}^{(1)}(\omega, \mathbf{x}')$  behaves approximately as an expanding spherical wave  $\sim \frac{e^{ikR'}}{R'}$  from a point source. This is consistent with our adopted interpretation of scattering as that from a small region on the surface of the Earth equal to the beam footprint; see Figure 2. We emphasize, though, that the complex amplitude of the scattered wave depends on the viewing

direction (3.28) (for  $\phi > 0$ ) via the arguments of  $\hat{\varepsilon}^{(1)}(\cdot)$  in (3.32). Hence, the field that propagates away from the target at different angles represents different Fourier components of the first order permittivity  $\varepsilon^{(1)}$  of (3.4). In particular, in the case of backscattering ( $\mathbf{x} = \mathbf{x}'$ ) we have  $\phi = \theta$  and  $\psi = \pi$  (see Figure 2), so that the Fourier component of  $\varepsilon^{(1)}$  substituted into (3.32) is  $\hat{\varepsilon}^{(1)}(0, -2k \sin \theta)$ . In the literature, the spatial frequency  $-2k \sin \theta$  is referred to as the Bragg (resonant) frequency—see, e.g., [3, section 13.1] or [17]—and accordingly,  $\hat{\varepsilon}^{(1)}(0, -2k \sin \theta)$  is the amplitude of the Bragg harmonic in the spectrum of  $\varepsilon^{(1)}$ .

We would also like to note that the approximations we have used for the incident and scattered fields (see formulae (3.1) and (3.32), respectively) are in some sense opposite. Whereas for the incident field we have fixed the propagation direction and replaced the spherical wave by a plane wave locally near the target, for the reflected field we are rather considering the propagation in all directions away from a small scattering region on the surface.

**3.4. Reflected field in the time domain.** To convert (3.32) back to the time domain, we first introduce a new set of Cartesian coordinates on the plane  $(\zeta_1, \zeta_2)$ :

$$(3.42) \quad \begin{aligned} \zeta'_1 &= \zeta_1 \sin \alpha + \zeta_2 \cos \alpha, \\ \zeta'_2 &= -\zeta_1 \cos \alpha + \zeta_2 \sin \alpha, \end{aligned}$$

where

$$\begin{aligned} \sin \alpha &= \frac{\sin \phi \sin \psi}{D}, & \cos \alpha &= \frac{\sin \phi \cos \psi - \sin \theta}{D}, \\ D^2 &= \sin^2 \phi \sin^2 \psi + (\sin \phi \cos \psi - \sin \theta)^2 = \sin^2 \phi + \sin^2 \theta - 2 \sin \phi \cos \psi \sin \theta. \end{aligned}$$

We note that as both  $0 < \theta < \frac{\pi}{2}$  and  $0 < \phi < \frac{\pi}{2}$ , we have  $D^2 = 0$  for  $\phi = \theta$  and  $\cos \psi = 1$ , which corresponds to specular reflection (see Figure 2), and  $D^2 > 0$  otherwise. Hence, specular reflection is the only case where transformation (3.42) degenerates. This case will be analyzed separately. In the meantime, we assume that  $D^2 > 0$ .

Denote by  $\hat{\varepsilon}_n^{(1)}$  the Fourier-transformed first order permittivity as a function of the new coordinates (3.42), so that  $\hat{\varepsilon}_n^{(1)}(\zeta'_1, \zeta'_2) = \hat{\varepsilon}^{(1)}(\zeta_1, \zeta_2)$ . Then, following (3.13a), we can write

$$(3.43) \quad \begin{aligned} \varepsilon^{(1)}(z_1, z_2) &= \frac{1}{(2\pi)^2} \iint \hat{\varepsilon}_n^{(1)}(\zeta'_1, \zeta'_2) e^{i((\zeta'_1 \sin \alpha - \zeta'_2 \cos \alpha)z_1 + (\zeta'_1 \cos \alpha + \zeta'_2 \sin \alpha)z_2)} d\zeta'_1 d\zeta'_2 \\ &= \frac{1}{(2\pi)^2} \iint \hat{\varepsilon}_n^{(1)}(\zeta'_1, \zeta'_2) e^{i(z_1 \sin \alpha + z_2 \cos \alpha)\zeta'_1 + (-z_1 \cos \alpha + z_2 \sin \alpha)\zeta'_2} d\zeta'_1 d\zeta'_2 \\ &= \frac{1}{(2\pi)^2} \iint \hat{\varepsilon}_n^{(1)}(\zeta'_1, \zeta'_2) e^{i(z'_1 \zeta'_1 + z'_2 \zeta'_2)} d\zeta'_1 d\zeta'_2 = \varepsilon_n^{(1)}(z'_1, z'_2), \end{aligned}$$

where the transformation between  $(z'_1, z'_2)$  and  $(z_1, z_2)$  is the same as (3.42).

Let us now recall that  $k = \omega/c$  and use the factor  $\hat{\varepsilon}^{(1)}(k \sin \phi \sin \psi, k \sin \phi \cos \psi - k \sin \theta)$

on the right-hand side of (3.32) to define a new function of time:

$$\begin{aligned}
\mathcal{E}^{(1)}(t) &\stackrel{\text{def}}{=} \frac{1}{2\pi} \int_{-\infty}^{\infty} \hat{\varepsilon}^{(1)}(k \sin \phi \sin \psi, k \sin \phi \cos \psi - k \sin \theta) e^{-i\omega t} d\omega \\
&= \frac{1}{2\pi} \int_{-\infty}^{\infty} \hat{\varepsilon}^{(1)}\left(\frac{\omega}{c} D \sin \alpha, \frac{\omega}{c} D \cos \alpha\right) e^{-i\omega t} d\omega \\
(3.44) \quad &= \frac{1}{2\pi} \int_{-\infty}^{\infty} \hat{\varepsilon}_n^{(1)}\left(\frac{\omega}{c} D, 0\right) e^{-i\omega t} d\omega = \frac{1}{2\pi} \frac{c}{D} \int_{-\infty}^{\infty} \hat{\varepsilon}_n^{(1)}(\omega', 0) e^{i\omega'(-ct/D)} d\omega' \\
&= \frac{c}{D} \int_{-\infty}^{\infty} \varepsilon_n^{(1)}\left(-\frac{ct}{D}, z'_2\right) dz'_2,
\end{aligned}$$

where the last equality in (3.44) is established with the help of (3.43). Note that it is precisely the specific choice of the coordinate transformation (3.42) that essentially makes  $\hat{\varepsilon}_n^{(1)}(\cdot)$  in (3.44) a function of only one argument and hence allows us to define  $\mathcal{E}^{(1)} = \mathcal{E}^{(1)}(t)$ . By construction,

$$\tilde{\mathcal{E}}^{(1)}(\omega) \stackrel{\text{def}}{=} \int_{-\infty}^{\infty} \mathcal{E}^{(1)}(t) e^{i\omega t} dt = \hat{\varepsilon}^{(1)}(k \sin \phi \sin \psi, k \sin \phi \cos \psi - k \sin \theta).$$

Therefore, we can recast formula (3.32) as follows:

$$(3.45) \quad \tilde{u}^{(1)}(\omega, \mathbf{x}') = -\frac{i\mathcal{M}(\varepsilon^{(0)}, \theta, \phi)}{4\pi^2 RR'} e^{i\frac{\omega}{c}(R+R')} \frac{\omega}{c} \tilde{P}(\omega) \tilde{\mathcal{E}}^{(1)}(\omega).$$

Next, we note that

$$-i\omega e^{i\frac{\omega}{c}(R+R')} \tilde{P}(\omega) = \int_{-\infty}^{\infty} P' \left( t - \frac{R+R'}{c} \right) e^{i\omega t} dt,$$

where  $P'$  is the first derivative of the function  $P$  with respect to its argument. Thus, on the right-hand side of (3.45) we have a product of two Fourier transforms, which means that the original function in the time domain, i.e.,  $u^{(1)}(t, \mathbf{x}')$ , can be represented as a convolution:

$$\begin{aligned}
u^{(1)}(t, \mathbf{x}') &= \frac{\mathcal{M}(\varepsilon^{(0)}, \theta, \phi)}{4\pi^2 RR'c} P' \left( t - \frac{R+R'}{c} \right) * \mathcal{E}^{(1)}(t) \\
&= \frac{\mathcal{M}(\varepsilon^{(0)}, \theta, \phi)}{4\pi^2 RR'c} \int P' \left( t - \frac{R+R'}{c} - t' \right) \mathcal{E}^{(1)}(t') dt' \\
(3.46) \quad &= \frac{\mathcal{M}(\varepsilon^{(0)}, \theta, \phi)}{4\pi^2 RR'c} \int P' \left( t - \frac{R+R'}{c} - t' \right) \frac{c}{D} \int \varepsilon_n^{(1)} \left( -\frac{ct'}{D}, z'_2 \right) dz'_2 dt' \\
&= \frac{\mathcal{M}(\varepsilon^{(0)}, \theta, \phi)}{4\pi^2 RR'c} \iint P' \left( t - \frac{R+R'}{c} + \frac{z'_1 D}{c} \right) \varepsilon_n^{(1)}(z'_1, z'_2) dz'_1 dz'_2 \\
&= \frac{\mathcal{M}(\varepsilon^{(0)}, \theta, \phi)}{4\pi^2 RR'c} \iint P' \left( t - \frac{\mathcal{R}_z + \mathcal{R}'_z}{c} \right) \varepsilon^{(1)}(z_1, z_2) dz_1 dz_2,
\end{aligned}$$

where we have substituted  $\mathcal{E}^{(1)}$  in the form given by the last integral of (3.44) and also changed the order of integration because the argument of  $P'(\cdot)$  does not depend on  $z'_2$ . The quantities

$\mathcal{R}_z$  and  $\mathcal{R}'_z$  in the last integral of (3.46) are the linearized travel distances between the location  $\mathbf{z}$  in the target area and the locations  $\mathbf{x}$  and  $\mathbf{x}'$  of the transmitting and receiving antennas, respectively (see Figure 2):

$$(3.47) \quad \begin{aligned} |\mathbf{z} - \mathbf{x}| &= R_z \approx \mathcal{R}_z \stackrel{\text{def}}{=} R + z_2 \sin \theta, \\ |\mathbf{z} - \mathbf{x}'| &= R'_z \approx \mathcal{R}'_z \stackrel{\text{def}}{=} R' - (z_1 \sin \phi \sin \psi + z_2 \sin \phi \cos \psi). \end{aligned}$$

Similarly to (3.1), in (3.47) we have dropped all the terms that are at least  $z_2/R$ ,  $z_1/R'$ , or  $z_2/R'$  smaller than the retained ones. For backscattering ( $\mathbf{x} = \mathbf{x}'$ ), formula (3.46) simplifies:

$$(3.46') \quad u^{(1)}(t, \mathbf{x}) = \frac{\mathcal{M}(\varepsilon^{(0)}, \theta, \theta)}{4\pi^2 R^2 c} \iint P' \left( t - 2 \frac{\mathcal{R}_z}{c} \right) \varepsilon^{(1)}(z_1, z_2) dz_1 dz_2.$$

In the case of specular reflection,  $\phi = \theta$  and  $\psi = 0$  (see Figure 2), the coordinate transformation (3.42) degenerates,  $D = 0$ , and hence we cannot introduce  $\mathcal{E}^{(1)}(t)$  according to (3.44). However, the reflected field given by (3.46) remains finite. In order to see that, we consider a formal limit  $D \rightarrow 0$  on the third and fourth lines of (3.46). After the change of variables  $z'_1 = ct/D$ , the only occurrence of  $D$  remains in the argument of  $P'(\cdot)$ . Taking the limit  $D \rightarrow 0$  implies that this argument will no longer depend on the spatial coordinates, and instead of (3.46) in the case of specular reflection we can write

$$u^{(1)}(t, \mathbf{x}') = \frac{\mathcal{M}(\varepsilon^{(0)}, \theta, \theta)}{4\pi^2 R R' c} P' \left( t - \frac{R + R'}{c} \right) \iint \varepsilon^{(1)}(z_1, z_2) dz_1 dz_2.$$

The fact that the time-delayed pulse  $P'(\cdot)$  can be taken out of the integral has a clear physical explanation. Indeed, in the case of specular reflection according to (3.47) we have

$$|\mathbf{z} - \mathbf{x}| + |\mathbf{z} - \mathbf{x}'| \approx \mathcal{R}_z + \mathcal{R}'_z = R + R' = \text{const};$$

i.e., the two-way travel distance remains approximately constant for the entire target area.

Formulae (3.46) and (3.46') are the counterparts of formulae (2.11') and (2.11''), respectively, obtained in the framework of the new model for radar targets that exploits a horizontally inhomogeneous material half-space (3.4). The function  $\varepsilon^{(1)}(z_1, z_2)$  in (3.46) and (3.46'), which is a counterpart of  $\nu(\mathbf{z})$  in (2.11') and (2.11''), is a function of only two variables by design. Therefore, unlike (2.11') and (2.11''), the new expressions (3.46) and (3.46') involve only surface convolutions (the integration is  $dz_1 dz_2$ ) and do not require any external considerations, such as the special singular form (2.22) for ground reflectivity, to reduce triple integrals to double integrals. In the literature, the convolutions that appear in (3.46) and (3.46') are referred to as surface retarded potentials. In addition, we emphasize that while the derivation of formulae (3.46) and (3.46') requires that the scattering be linearized, it does not require that it should be weak, and does not employ the first Born approximation.

Alternative scattering models based on different physical considerations can also be used. For example, the impedance boundary condition model (see Appendix B), which is, however, not as rigorously justified as the model presented in this section, yields a reflection coefficient similar to (3.22); see (B.8). With slight modifications (in particular, with a modified function  $\mathcal{M}$  of (3.33)), the rest of the analysis will apply to this model as well. Yet another model which may be useful is scattering off a rough surface; see, e.g., [31]. For small perturbations of the surface, it can also produce a reflection coefficient of type (3.22).

**4. SAR ambiguity theory for the new scattering model.** The SAR ambiguity theory for the target model of section 3 can be developed similarly to the conventional construction of section 2.1. The development in the new framework is even more straightforward, as it does not involve any artificial steps aimed at interpreting the ground reflectivity as a function of only two rather than three spatial variables. As in section 2.1, we will restrict our considerations to the case of monostatic imaging, for which the first order scattered field is given by formula (3.46'). Moreover, in this section we will separate the scales in both the imaged quantity and the image and show that the actual SAR observable quantity is a slowly varying amplitude of the Bragg harmonic of  $\varepsilon^{(1)}$ . Hereafter, we will assume that  $\mathbf{z} = (z_1, z_2, 0)$ ,  $\mathbf{y} = (y_1, y_2, 0)$ , and  $d\mathbf{z} = dz_1 dz_2$ . Then, in particular, we can say that  $\varepsilon^{(1)}(z_1, z_2) = \varepsilon^{(1)}(\mathbf{z})$  and recast the surface convolution (3.46') as follows:

$$(3.46'') \quad u^{(1)}(t, \mathbf{x}) = \frac{\mathcal{M}(\varepsilon^{(0)}, \theta, \theta)}{4\pi^2 R^2 c} \iint P' \left( t - 2\frac{\mathcal{R}_z}{c} \right) \varepsilon^{(1)}(\mathbf{z}) d\mathbf{z}.$$

For the satellite at the position  $\mathbf{x}$ , using (3.46'') instead of (2.11''), we then get (cf. (2.13))

$$\begin{aligned} I_{\mathbf{x}}(\mathbf{y}) &= \int_{\chi} \overline{P(t - 2\mathcal{R}_y/c)} u^{(1)}(t, \mathbf{x}) dt \\ &= \frac{\mathcal{M}(\varepsilon^{(0)}, \theta, \theta)}{4\pi^2 R^2 c} \iint d\mathbf{z} \varepsilon^{(1)}(\mathbf{z}) \int_{\chi} dt \overline{P(t - 2\mathcal{R}_y/c)} P'(t - 2\mathcal{R}_z/c), \end{aligned}$$

where  $\mathcal{R}_y$  is the linearized distance  $|\mathbf{y} - \mathbf{x}|$  defined as in (3.47). Then, taking into account that  $P' \approx -i\omega_0 P$ , we arrive at the same formal expression for the image as (2.15),

$$(2.15') \quad I_{\mathbf{x}}(\mathbf{y}) = \iint W_{\mathbf{x}}(\mathbf{y}, \mathbf{z}) \nu(\mathbf{z}) d\mathbf{z},$$

except that the integral is two-dimensional by construction and does not require assumption (2.22). In formula (2.15'),

$$(4.1) \quad \begin{aligned} \nu(\mathbf{z}) &= -i\omega_0 \frac{\mathcal{M}(\varepsilon^{(0)}, \theta, \theta)}{4\pi^2 R^2 c} \varepsilon^{(1)}(\mathbf{z}) \quad \text{and} \\ W_{\mathbf{x}}(\mathbf{y}, \mathbf{z}) &= \tau \operatorname{sinc} \left( \pi \frac{\mathcal{R}_z - \mathcal{R}_y}{\Delta_R} \right) e^{2ik_0(\mathcal{R}_z - \mathcal{R}_y)} = W_R(\mathbf{y}, \mathbf{z}) e^{2ik_0(\mathcal{R}_z - \mathcal{R}_y)}, \end{aligned}$$

where  $W_R(\mathbf{y}, \mathbf{z})$  in the form of a sinc function is obtained as in Appendix A; see (A.1), (A.2).

Consider  $\mathbf{x} = \mathbf{x}^0$ , so that

$$\mathcal{R}_z - \mathcal{R}_y \equiv \mathcal{R}_z^0 - \mathcal{R}_y^0 = (z_2 - y_2) \sin \theta.$$

Then, from (2.15') and (4.1) we have

$$(4.2) \quad I_{\mathbf{x}^0}(\mathbf{y}) = \tau \int dz_1 \int dz_2 \operatorname{sinc} \left( \pi \frac{(z_2 - y_2) \sin \theta}{\Delta_R} \right) e^{2ik_0(z_2 - y_2) \sin \theta} \nu(z_1, z_2).$$

In general, for  $\mathbf{x} = \mathbf{x}^n$  the difference of two linearized travel distances is given by (A.3):

$$\mathcal{R}_z - \mathcal{R}_y \equiv \mathcal{R}_z^n - \mathcal{R}_y^n = (z_2 - y_2) \sin \theta + \frac{y_1 - z_1}{R} x_1^n.$$

As  $|x_1^n| \ll R$ , we may neglect the term with  $x_1^n$  in the argument of the  $\text{sinc}(\cdot)$  in (4.1):

$$(4.3) \quad \text{sinc} \left( \pi \sin \theta \frac{z_2 - y_2}{\Delta_R} + \pi \frac{x_1^n}{R} \frac{y_1 - z_1}{\Delta_R} \right) \approx \text{sinc} \left( \pi \sin \theta \frac{z_2 - y_2}{\Delta_R} \right) = \text{sinc} \left( \pi \frac{\mathcal{R}_z^0 - \mathcal{R}_y^0}{\Delta_R} \right)$$

(see [15, Appendix A] for a detailed analysis). This term, however, should be retained in the exponent, as it is responsible for the chirp-type behavior in azimuth and hence for obtaining the azimuthal resolution; see Appendix A. Therefore, we get (cf. (2.16))

$$(4.4) \quad \begin{aligned} I(\mathbf{y}) &= \sum_{n=-N/2}^{N/2} I_{x^n}(\mathbf{y}) = \tau \int dz_1 \sum_{n=-N/2}^{N/2} e^{2ik_0 x_1^n (y_1 - z_1)/R} \nu_w(z_1, y_2) \\ &= \tau \int dz_1 W_A(y_1, z_1) \nu_w(z_1, y_2), \end{aligned}$$

where  $W_A(y_1, z_1)$  is given by (2.24b) and  $\nu_w(z_1, y_2)$  is the interior convolution integral on the right-hand side of formula (4.2):

$$(4.5) \quad \nu_w(z_1, y_2) \stackrel{\text{def}}{=} \int W_R(y_2 - z_2) e^{-2ik_0(y_2 - z_2) \sin \theta} \cdot \nu(z_1, z_2) dz_2.$$

In (4.5), we took into account that  $\text{sinc}$  is an even function. Note also that unlike in (2.12'), (2.22), the quantity  $\nu(\mathbf{z})$  in (4.1), (4.5) depends, in particular, on the angle of incidence  $\theta$ .

Representations (4.2), (4.4), and (4.5) will allow us to separate the fast ( $\sim k_0^{-1}$ , the wavelength) and slow ( $\sim \Delta_R$ , the resolution, which is much larger than the wavelength,  $\Delta_R \gg k_0^{-1}$ ) scales of variation in both the imaged quantity and the image. As a result, we will be able to identify a slowly varying physical observable for the new scattering model. It will replace  $\nu$  in relation (2.16) and provide a new characteristic of the target that will generate the image once processed with the slowly varying generalized ambiguity function.

On the one hand, taking the Fourier transform in  $y_2$  of both sides of (4.5), we get

$$(4.6) \quad \hat{\nu}_w(z_1, k) = \tau \frac{\Delta_R}{\sin \theta} \hat{\nu}(z_1, k) \chi_\beta(k - k_\theta),$$

where  $k_\theta$  is the Bragg frequency,

$$(4.7) \quad k_\theta = -2k_0 \sin \theta,$$

and the indicator function  $\chi_\beta$  is defined as in (2.9), but for  $\beta = \frac{2\pi \sin \theta}{\Delta_R} = \frac{2B \sin \theta}{c}$ :

$$(4.8) \quad \chi_\beta(k - k_\theta) = \begin{cases} 1 & \text{if } k \in [k_\theta - \frac{B \sin \theta}{c}, k_\theta + \frac{B \sin \theta}{c}] , \\ 0 & \text{otherwise.} \end{cases}$$

To obtain (4.6), we took into account that the right-hand side of (4.5) is a convolution and that for the Fourier transform of the first factor in this convolution (see (4.1)) we have

$$\begin{aligned} &\tau \int \text{sinc} \left( \pi \frac{z \sin \theta}{\Delta_R} \right) e^{-i2k_0 \sin \theta z} e^{-ikz} dz = \hat{W}_R(2k_0 \sin \theta + k) \\ &= \tau \frac{\Delta_R}{\sin \theta} \chi_\beta(2k_0 \sin \theta + k) = \tau \frac{\Delta_R}{\sin \theta} \chi_\beta(k - k_\theta). \end{aligned}$$

Formulae (4.6)–(4.8) show that  $\nu_w(z_1, y_2)$  of (4.5) is a band limited function. Its spectrum contains only the interval of spatial frequencies of size  $\beta = \frac{2B \sin \theta}{c}$  centered at the Bragg frequency (4.7). Hence, without changing the image (4.4), the function  $\nu(z_1, z_2)$  on the right-hand side of (4.5) can be replaced with an effective function  $\nu^{\text{eff}}(z_1, z_2)$  such that its spectrum in  $z_2$  is restricted to the same band as in (4.8),  $\hat{\nu}^{\text{eff}}(z_1, k) \stackrel{\text{def}}{=} \hat{\nu}(z_1, k) \chi_\beta(k - k_\theta)$ :

$$(4.9) \quad \nu^{\text{eff}}(z_1, z_2) \stackrel{\text{def}}{=} \frac{1}{2\pi} \int_{k_\theta - \beta/2}^{k_\theta + \beta/2} \hat{\nu}(z_1, k) e^{ikz_2} dk.$$

Both  $\nu_w(z_1, y_2)$  of (4.5) and  $\nu^{\text{eff}}(z_1, z_2)$  are band limited on the spectral interval  $[k_\theta - \frac{\beta}{2}, k_\theta + \frac{\beta}{2}]$ .

On the other hand, taking into account (4.9), we can recast formula (4.5) as

$$e^{2ik_0 y_2 \sin \theta} \nu_w(z_1, y_2) = \int W_R(y_2 - z_2) e^{2ik_0 z_2 \sin \theta} \nu^{\text{eff}}(z_1, z_2) dz_2,$$

and then introduce the new functions on both the left-hand and right-hand sides of the previous equality:

$$(4.10a) \quad \nu_w^{\text{new}}(z_1, y_2) \stackrel{\text{def}}{=} e^{2ik_0 y_2 \sin \theta} \nu_w(z_1, y_2),$$

$$(4.10b) \quad \nu^{\text{new}}(z_1, z_2) \stackrel{\text{def}}{=} e^{2ik_0 z_2 \sin \theta} \nu^{\text{eff}}(z_1, z_2),$$

so that

$$(4.5') \quad \nu_w^{\text{new}}(z_1, y_2) = \int W_R(y_2 - z_2) \nu^{\text{new}}(z_1, z_2) dz_2 \equiv W_R * \nu^{\text{new}}.$$

Fourier transforming both sides of (4.5') in  $y_2$ , we obtain (cf. (4.6))

$$(4.6') \quad \hat{\nu}_w^{\text{new}}(z_1, k) = \hat{\nu}_w(z_1, k + k_\theta) = \tau \frac{\Delta_R}{\sin \theta} \hat{\nu}^{\text{new}}(z_1, k) \chi_\beta(k),$$

where according to (4.9) and (4.10b),

$$(4.11) \quad \hat{\nu}^{\text{new}}(z_1, k) = \hat{\nu}^{\text{eff}}(k + k_\theta) = \hat{\nu}(z_1, k + k_\theta) \chi_\beta(k).$$

From (4.6') and (4.11) we conclude that, similarly to  $\nu_w(z_1, y_2)$  and  $\nu^{\text{eff}}(z_1, z_2)$ , both the function  $\nu_w^{\text{new}}(z_1, y_2)$  of (4.10a) and the function  $\nu^{\text{new}}(z_1, z_2)$  of (4.10b) are band limited to a spectral interval of size  $\beta$ . However, while for  $\nu_w(z_1, y_2)$  and  $\nu^{\text{eff}}(z_1, z_2)$  we have

$$\hat{\nu}_w(z_1, k) \neq 0 \quad \text{and} \quad \hat{\nu}^{\text{eff}}(z_1, k) \neq 0 \quad \text{if} \quad k \in \left[ k_\theta - \frac{\beta}{2}, k_\theta + \frac{\beta}{2} \right],$$

the spectral interval for the new functions  $\nu_w^{\text{new}}(z_1, y_2)$  and  $\nu^{\text{new}}(z_1, z_2)$  is centered at 0 rather than at the Bragg frequency  $k_\theta$  of (4.7):

$$\hat{\nu}_w^{\text{new}}(z_1, k) \neq 0 \quad \text{and} \quad \hat{\nu}^{\text{new}}(z_1, k) \neq 0 \quad \text{if} \quad k \in \left[ -\frac{\beta}{2}, \frac{\beta}{2} \right].$$

In other words, the new spectral interval is shifted by  $-k_\theta$ . Therefore, both  $\nu_w^{\text{new}}(z_1, y_2)$  of (4.10a) as a function of  $y_2$  and  $\nu^{\text{new}}(z_1, z_2)$  of (4.10b) as a function of  $z_2$  vary slowly in space, on the scale  $\sim \Delta_R$  or larger. Indeed, according to (4.6') and (4.11), none of the spatial frequencies in their respective spectra exceeds  $\beta/2 = B \sin \theta/c$ , which is assumed much smaller than the absolute Bragg frequency  $2k_0 \sin \theta$ . In other words,  $B/c \ll k_0$  or  $B \ll \omega_0$ , which is equivalent to assuming that the original SAR interrogating waveform (2.8) is narrow-band.

Given that the functions  $\nu_w^{\text{new}}(z_1, y_2)$  and  $\nu^{\text{new}}(z_1, z_2)$  vary in space on the scale of  $\Delta_R$  or slower, we redefine  $I_{\mathbf{x}^0}(\mathbf{y})$  of (4.2), as well as all  $I_{\mathbf{x}^n}(\mathbf{y})$ , by essentially absorbing the factor  $e^{2ik_0 y_2 \sin \theta}$  into the image, as in (4.5')

$$I_{\mathbf{x}^0}^{\text{new}}(\mathbf{y}) \stackrel{\text{def}}{=} e^{2ik_0 y_2 \sin \theta} I_{\mathbf{x}^0}(\mathbf{y}) = \tau \int dz_1 \int dz_2 W_R(y_2 - z_2) \nu^{\text{new}}(z_1, z_2) = \tau \int \nu_w^{\text{new}}(z_1, y_2) dz_1.$$

Then, assuming that  $\nu^{\text{new}}(z_1, z_2)$  does not depend on  $\mathbf{x}$ , for the full image (4.4) we obtain

$$\begin{aligned} I^{\text{new}}(\mathbf{y}) &= \sum_{n=-N/2}^{N/2} I_{\mathbf{x}^n}^{\text{new}}(\mathbf{y}) = \tau \int dz_1 \sum_{n=-N/2}^{N/2} e^{2ik_0 x_1^n (y_1 - z_1)/R} \nu_w^{\text{new}}(z_1, y_2) \\ (4.12) \qquad &= \int dz_1 \int dz_2 W_A(y_1, z_1) W_R(y_2, z_2) \nu^{\text{new}}(z_1, z_2) \\ &= W'(\mathbf{y}, \mathbf{z}) * \nu^{\text{new}}(\mathbf{z}). \end{aligned}$$

The function  $W'(\mathbf{y}, \mathbf{z}) = W_A(\mathbf{y}, \mathbf{z}) W_R(\mathbf{y}, \mathbf{z})$  in (4.12) is the same GAF as in (2.26), but without the fast phase factor  $e^{i\Phi_0} = e^{2ik_0(z_2 - y_2) \sin \theta}$ . Expression (4.12) is a counterpart of (2.16). Thus, we conclude that the new function  $\nu^{\text{new}}(\mathbf{z})$  represents the slowly varying observable quantity for the SAR imaging scheme that includes the target model of section 3.

According to (4.11), the new function  $\nu^{\text{new}}$  is obtained by shifting and band limiting (i.e., truncating by a rectangular window) the spectrum of the original function  $\nu$ . In fact,  $\nu^{\text{new}}$  can also be represented as a windowed Fourier transform (WFT; see, e.g., [18, Chapter 2]):

$$\begin{aligned} \nu^{\text{new}}(z_1, z_2) &= \frac{1}{2\pi} \int \hat{\nu}(z_1, k + k_\theta) \chi_\beta(k) e^{ikz_2} dk \\ &= \frac{1}{2\pi} \int \hat{\nu}(z_1, k + k_\theta) \left( \frac{\tau \sin \theta}{\Delta_R} \int W_R(z) e^{-ikz} dz \right) e^{ikz_2} dk \\ (4.13) \qquad &= \frac{\tau \sin \theta}{2\pi \Delta_R} \int W_R(z) \int \hat{\nu}(z_1, k + k_\theta) e^{ik(z_2 - z)} dk dz \\ &= \frac{\tau \sin \theta}{2\pi \Delta_R} \int W_R(z) \int \hat{\nu}(z_1, k') e^{i(k' - k_\theta)(z_2 - z)} dk' dz \\ &= \frac{\tau \sin \theta}{2\pi \Delta_R} \int W_R(z_2 - z') \int \hat{\nu}(z_1, k') e^{i(k' - k_\theta)z'} dk' dz' \\ &= \frac{\tau \sin \theta}{\Delta_R} \int W_R(z_2 - z') e^{-ik_\theta z'} \left( \frac{1}{2\pi} \int \hat{\nu}(z_1, k') e^{ik' z'} dk' \right) dz' \\ &= \frac{\tau \sin \theta}{\Delta_R} \int W_R(z_2 - z') \nu(z_1, z') e^{-ik_\theta z'} dz'. \end{aligned}$$

Formula (4.13) enables a convenient physical interpretation of the observable  $\nu^{\text{new}}$ . This quantity appears to be a WFT of  $\nu(z_1, z')$  with respect to its second argument  $z'$ , with a sinc window of size  $\frac{\Delta_R}{\sin \theta}$  centered at  $z_2$  and precisely the Bragg spatial frequency (4.7). In other words,  $\nu^{\text{new}}(z_1, z_2)$  as a function of  $z_2$  is a slowly varying amplitude of the Bragg harmonic  $e^{ik_\theta z_2}$  in the spectrum of  $\nu$  computed on a window of the resolution size.

We also need to emphasize that the independence of  $\nu^{\text{new}}(z_1, z_2)$  on  $\mathbf{x}$  that enables representation (4.12) can only be considered an approximation. Indeed, the left-hand side of (4.3) depends on the position  $\mathbf{x}^n$  of the SAR platform, and so does  $I_{\mathbf{x}^n}(\mathbf{y})$ . Consequently, the dependence on  $n$  may need to be taken into account on the right-hand side of (4.5'), which will eventually translate into the dependence of  $\nu^{\text{new}}(z_1, z_2)$  on  $n$ . Alternatively, one can think that the WFT in (4.13) is performed along slightly different directions for different positions of the platform. For narrow-angle synthetic apertures the corresponding variation of the observable quantity is small and can be disregarded. This is equivalent to dropping the term  $\propto x_1^n$  in the argument of the sinc  $(\cdot)$  in (4.3). For wider apertures, however, taking the WFT along different directions may lead to a reduction or loss of the spatial (or angular) coherence. This issue will require thorough attention in the future.

Finally, the analysis in this section indicates that the same interpretation of the observable quantity in SAR imaging, i.e., the interpretation as a slowly varying amplitude of the Bragg harmonic in the spectrum of ground reflectivity, may potentially be extended to the conventional SAR ambiguity theory as well (section 2.1 and Appendix A).

**5. Conclusions and future work.** We have proposed a new model for radar targets that exploits a horizontally inhomogeneous dielectric half-space; see the beginning of section 3 and also (3.4). In the framework of this model, one can consider the linearized scattering without assuming that it is weak. This enables the development of a SAR ambiguity theory that does not require the first Born approximation. Moreover, an intrinsic property of the new model is that it represents the scattered field as a surface (rather than volumetric) retarded potential; see (3.46) and (3.47). This allows one to avoid making additional assumptions, such as taking the ground reflectivity as a single layer on the surface, that may be inconsistent with other parts of the formulation. Finally, the new model helps identify the correct physical observable for SAR imaging. It is a slowly varying amplitude of the Bragg resonant harmonic in the spectrum of electric permittivity computed on a resolution size window; see (4.13). Note that the variation of the medium on the resonant Bragg scale makes our model distinctly different from those that appear in the context of imaging through a randomly layered medium, in which one often employs homogenization and requires that the typical incident wavelength be much larger than the characteristic scale of variation of the medium parameters; see, e.g., [10, Chapter 4] or [11]. Another important difference between our formulation and that of [10, 11] is that we allow variations of the medium in two spatial directions.

Altogether, our new scattering model allows one to address a broader class of problems than the conventional SAR theory does, because the linearization can be performed against a different background solution rather than only the unobstructed incident field in free space, as in the case of weak scattering. However, when the scattering is indeed weak, the results obtained with the help of the new model become fully equivalent to those from the classical theory.

In the current paper, we have considered only the scalar case. This is a simplified setting, because in reality the electric and magnetic fields are vector quantities, and scattering of electromagnetic waves needs to be analyzed using full Maxwell's equations as opposed to the d'Alembert equation (2.1). In the case of specular reflection, linearized scattering off an anisotropic dielectric and weakly conducting half-space was studied in [13]. For planar scattering (when the reflected wave vector is in the plane of incidence), the formulation we have described in this paper corresponds to the horizontal polarization of the electric field (the electric field vector is parallel to the surface). To address vertical polarization, one should start the analysis with full Maxwell's equations that can subsequently be reduced to scalar second order equations for individual field components, but both the equations and the interface conditions will be somewhat different from those considered in this paper. The analysis of nonplanar scattering requires a full vector consideration that would involve computing two co-polarized and two cross-polarized scattering coefficients (a  $2 \times 2$  scattering matrix altogether). Both the case of vertical polarization and that of nonplanar scattering will be included in our forthcoming monograph [16].

The SAR ambiguity theory actually relies on the spatial (or angular) coherence of the scattering of radar signals off the target. In the conventional framework of section 2.1, coherence manifests itself as independence of the scattering coefficient  $\nu(\mathbf{z})$  given by (2.12') from the antenna position  $\mathbf{x}$ . It is this property of the scattering coefficient that allows one to represent the image as a convolution of  $\nu(\mathbf{z})$  with the GAF  $W(\mathbf{y}, \mathbf{z})$  (see (2.16)), where  $W(\mathbf{y}, \mathbf{z})$  characterizes only the imaging system and not the target (in particular,  $W(\mathbf{y}, \mathbf{z})$  depends on the array of the antenna positions  $\{\mathbf{x}^n\}$  that form the synthetic aperture). For the new model, an equivalent requirement would be independence of the slowly varying observable quantity  $\nu^{\text{new}}(z_1, z_2)$  from  $\mathbf{x}$  or from  $n$ , as discussed in section 4. For narrow synthetic apertures this assumption may approximately hold, but for wider aperture angles it becomes unrealistic; see, e.g., [23, 2, 27]. The mechanism of coherence deterioration can be attributed to the leftmost expression of (4.3), where the azimuthal coordinates get "mixed" into the range factor of the convolution kernel. Alternatively, one can think of performing the WFT (4.2) along different directions for different antenna positions.

Given that coherence is critical for SAR imaging, two directions of the future study are warranted. On the one hand, quantitative estimates will need to be obtained for the maximum aperture angles that would still allow the use of coherence in SAR analysis, and that would relate the gradual deterioration of coherence due to wider apertures to the anticipated overall degradation of the SAR performance. Note that the second term in the argument of the  $\text{sinc}(\cdot)$  on the left-hand side of (4.3), which is responsible for coherence deterioration, is what actually needs to be taken into account when estimating the error due to the factorization (2.19); see [15, Appendix A]. On the other hand, it would be interesting to try and identify the classes of targets for which the scattering will remain coherent even for wider apertures. For example, a sufficient condition would be to have a target for which the result of the WFT (4.2) will not depend on the direction.

In this paper we have generalized the linearized scattering model beyond the first Born approximation by considering linearization against a different background solution—transmission/scattering of a plane wave at a planar interface between the vacuum and a homogeneous dielectric with a potentially large permittivity  $\varepsilon^{(0)}$ . In the future, it may be interesting to

consider other background solutions for linearization, for example, transmission/scattering at an interface of a different shape.

Other possible extensions of the current work include relaxing the assumption that the ground topography be flat, which is intrinsic in formula (3.4), and investigating whether and how the proposed methodology can be generalized to the case of a nonplanar (yet known) surface of the target, as well as conducting SAR ambiguity analysis for platform trajectories that are more general than the linear flight path (orbit) at a constant altitude (as in Figures 1 and 2).

**Appendix A. Computation of the GAF (2.19).** The range factor (2.21) of the GAF is given by

$$\begin{aligned} W_{\mathbf{R}}(\mathbf{y}, \mathbf{z}) &= \int_{\chi} \overline{A(t - 2R_{\mathbf{y}}^0/c)} A(t - 2R_{\mathbf{z}}^0/c) dt \\ &= \int_{\chi} \chi_{\tau}(t - 2R_{\mathbf{y}}^0/c) e^{i\alpha(t - 2R_{\mathbf{y}}^0/c)^2} \chi_{\tau}(t - 2R_{\mathbf{z}}^0/c) e^{-i\alpha(t - 2R_{\mathbf{z}}^0/c)^2} dt \\ &= \int_{\max\{2R_{\mathbf{y}}^0/c, 2R_{\mathbf{z}}^0/c\} - \tau/2}^{\min\{2R_{\mathbf{y}}^0/c, 2R_{\mathbf{z}}^0/c\} + \tau/2} e^{i\alpha(t - 2R_{\mathbf{y}}^0/c)^2} e^{-i\alpha(t - 2R_{\mathbf{z}}^0/c)^2} dt. \end{aligned}$$

In the last integral, we change the integration variable,  $\tilde{t} = t - (R_{\mathbf{y}}^0 + R_{\mathbf{z}}^0)/c$ , and also denote  $T^0 = (R_{\mathbf{y}}^0 - R_{\mathbf{z}}^0)/c$  so that

$$t - \frac{2R_{\mathbf{y}}^0}{c} = \tilde{t} - T^0 \quad \text{and} \quad t - \frac{2R_{\mathbf{z}}^0}{c} = \tilde{t} + T^0.$$

Then, we have

$$(A.1) \quad W_{\mathbf{R}}(\mathbf{y}, \mathbf{z}) = \int_{-\tau/2 + |T^0|}^{\tau/2 - |T^0|} e^{i\alpha(\tilde{t} - T^0)^2} e^{-i\alpha(\tilde{t} + T^0)^2} d\tilde{t} = \int_{-\tilde{\tau}/2}^{\tilde{\tau}/2} e^{-i\alpha 4\tilde{t}T^0} d\tilde{t},$$

where  $\tilde{\tau} = \tau - 2|T^0|$ . Consequently,

$$\begin{aligned} (A.2) \quad W_{\mathbf{R}}(\mathbf{y}, \mathbf{z}) &= -\frac{1}{4i\alpha T^0} \left( e^{-2i\alpha\tilde{\tau}T^0} - e^{2i\alpha\tilde{\tau}T^0} \right) = \frac{\sin(2\alpha\tilde{\tau}T^0)}{2\alpha T^0} \\ &= \tilde{\tau} \operatorname{sinc}(2\alpha\tilde{\tau}T^0) = \tilde{\tau} \operatorname{sinc} \left( \frac{B}{\tau} \tilde{\tau} \frac{R_{\mathbf{y}}^0 - R_{\mathbf{z}}^0}{c} \right) \\ &\approx \tau \operatorname{sinc} \left( \frac{B}{c} (R_{\mathbf{y}}^0 - R_{\mathbf{z}}^0) \right) = \tau \operatorname{sinc} \left( \pi \frac{R_{\mathbf{y}}^0 - R_{\mathbf{z}}^0}{\Delta_{\mathbf{R}}} \right), \end{aligned}$$

where  $\Delta_{\mathbf{R}} = \pi c/B$ . Note that in the last line of (A.2) we have replaced  $\tilde{\tau}$  by  $\tau$ . This was done because  $|T^0| \ll \tau$ , and hence the two quantities,  $\tilde{\tau}$  and  $\tau$ , are very close to each other. Indeed,  $|T^0|$  is the signal travel time between  $\mathbf{y}$  and  $\mathbf{z}$  (see Figure 1), which is several orders of magnitude shorter than the typical duration of the pulse  $\tau$  (see [14, Table 1]).

The sinc function in (A.2) attains its maximum when  $R_{\mathbf{y}}^0 = R_{\mathbf{z}}^0$  and has its first zero when  $R_{\mathbf{y}}^0 - R_{\mathbf{z}}^0 = \Delta_{\mathbf{R}}$ . Therefore,  $\Delta_{\mathbf{R}}$  is the semiwidth of the main lobe of the sinc. In the

literature, the quantity  $\Delta_R = \pi c/B$  is commonly interpreted as the range resolution, because it is assumed that if two point targets are at least  $\Delta_R$  apart, then their images given by sinc functions of semiwidth  $\Delta_R$  can be distinguished from one another.

To evaluate the azimuthal factor (2.20), we first linearize the travel distances  $R_{\mathbf{y}}^n$  and  $R_{\mathbf{z}}^n$  of (2.18); see Figure 1. With no loss of generality we can assume that  $z_2 = 0$  and also denote  $y_2 - z_2 = y_2 = l$  for convenience. Then, we can write

$$\begin{aligned} R_{\mathbf{z}}^n &= (H^2 + L^2 + (x_1^n - z_1)^2)^{1/2} = (R^2 + (x_1^n - z_1)^2)^{1/2} \\ &= R \left( 1 + \frac{(x_1^n - z_1)^2}{R^2} \right)^{1/2} \approx R + \frac{1}{2} \frac{(x_1^n - z_1)^2}{R} \end{aligned}$$

and

$$\begin{aligned} R_{\mathbf{y}}^n &= (H^2 + (L + l)^2 + (x_1^n - y_1)^2)^{1/2} = (R^2 + 2Ll + l^2 + (x_1^n - y_1)^2)^{1/2} \\ &= R \left( 1 + \frac{2Ll + l^2 + (x_1^n - y_1)^2}{R^2} \right)^{1/2} \approx R + \frac{1}{2} \frac{2Ll + l^2 + (x_1^n - y_1)^2}{R}, \end{aligned}$$

where  $|x_1^n - y_1| \sim L_{\text{SA}}$ ,  $|x_1^n - z_1| \sim L_{\text{SA}}$ , and both  $L_{\text{SA}} \ll R$  and  $l \ll R$  (see [14, Table 1];  $l$  is on the order of resolution). Subtracting the previous equalities from one another, we obtain

$$(A.3) \quad R_{\mathbf{z}}^n - R_{\mathbf{y}}^n \approx \frac{(x_1^n - z_1)^2 - 2Ll - l^2 - (x_1^n - y_1)^2}{2R} \approx -\frac{Ll}{R} + \frac{(y_1 - z_1)x_1^n}{R},$$

where only the leading term was retained among those that do not depend on  $n$  (typically,  $l \ll L_{\text{SA}}$ ). Consequently, taking into account that  $x_1^n = L_{\text{SA}}n/N$ , for the sum (2.20) we have

$$\begin{aligned} (A.4) \quad W_{\Sigma}(\mathbf{y}, \mathbf{z}) &= \sum_{n=-N/2}^{N/2} e^{2ik_0(R_{\mathbf{z}}^n - R_{\mathbf{y}}^n)} = e^{-2ik_0Ll/R} \sum_{n=-N/2}^{N/2} e^{2ik_0(y_1 - z_1)x_1^n/R} \\ &= e^{-2ik_0Ll/R} \sum_{n=-N/2}^{N/2} e^{2ik_0(y_1 - z_1)L_{\text{SA}}n/RN} \\ &= e^{-2ik_0Ll/R} \frac{e^{-ik_0(y_1 - z_1)L_{\text{SA}}/R} - e^{ik_0(y_1 - z_1)L_{\text{SA}}(N+2)/RN}}{1 - e^{2ik_0(y_1 - z_1)L_{\text{SA}}/RN}}. \end{aligned}$$

For the common imaging configurations (see [14, Table 1]) we have  $k_0L_{\text{SA}}/N \gtrsim 1$ , whereas  $|y_1 - z_1|/R$  could be between  $10^{-5}$  and  $10^{-6}$ . Therefore, the exponent in the denominator of the last fraction is small:  $|2k_0(y_1 - z_1)L_{\text{SA}}/RN| \ll 1$ . Moreover,  $N \gg 1$ , and we can neglect  $2/N$  in the second exponent in the numerator. Hence, we get

$$\begin{aligned} (A.5) \quad W_{\Sigma}(\mathbf{y}, \mathbf{z}) &\approx e^{-2ik_0Ll/R} \frac{\sin(k_0(y_1 - z_1)L_{\text{SA}}/R)}{k_0(y_1 - z_1)L_{\text{SA}}/RN} \\ &= e^{-2ik_0Ll/R} N \text{sinc}(k_0(y_1 - z_1)L_{\text{SA}}/R) \\ &= e^{-2ik_0Ll/R} N \text{sinc}\left(\pi \frac{y_1 - z_1}{\Delta_A}\right) = e^{-2ik_0Ll/R} W_A(\mathbf{y}, \mathbf{z}), \end{aligned}$$

where  $\Delta_A = \pi R/k_0 L_{SA} = \pi Rc/\omega_0 L_{SA}$ . The same argument as in the case of range resolution allows one to take the quantity  $\Delta_A$  as the azimuthal resolution.

The fact that both  $W_R(\mathbf{y}, \mathbf{z})$  (see (A.2)) and  $W_A(\mathbf{y}, \mathbf{z})$  (see (A.5)) evaluate to a sinc function is not accidental. For the range factor  $W_R(\mathbf{y}, \mathbf{z})$  the sinc comes as an implication of the linear variation of the instantaneous frequency along the chirp (see (2.8) and (2.9)):  $\omega(t) = \omega_0 + 2\alpha t = \omega_0 + \frac{B}{\tau}t$ , where  $t \in [-\tau/2, \tau/2]$ , so that integral (A.1) can be recast as

$$(A.6) \quad W_R(\mathbf{y}, \mathbf{z}) = \int_{-\tilde{\tau}/2}^{\tilde{\tau}/2} e^{-2i(\omega(\tilde{t})-\omega_0)T^0} d\tilde{t}.$$

As for the azimuthal factor  $W_A(\mathbf{y}, \mathbf{z})$ , the exponents under the sum in (A.4) can be thought of as representing a linear variation of the local wavenumber along the synthetic array. Indeed, the quantity  $k(n) \stackrel{\text{def}}{=} k_0 L_{SA} n / RN$  depends linearly on  $n$ , and from (A.4) we have

$$(A.7) \quad W_A(\mathbf{y}, \mathbf{z}) = \sum_{n=-N/2}^{N/2} e^{2ik(n)(y_1-z_1)},$$

which is very similar to (A.6), because  $y_1 - z_1$  can substitute for  $T^0 \propto (R_{\mathbf{y}}^0 - R_{\mathbf{z}}^0)$ , and  $k(n)$  is a linear function of  $n$  that turns into zero exactly in the middle of the synthetic array, much like  $\omega(\tilde{t}) - \omega_0$  turns into zero in the middle of the chirp. The difference between (A.6) and (A.7) is that the former is an integral and the latter is a sum, but a sum of type (A.7) can always be thought of as approximating the corresponding integral by the midpoint rule.

Moreover, the ‘‘instantaneous’’ wavenumber  $k(n)$  can be recast as follows:

$$(A.8) \quad k(n) = k_0 \frac{x_1^n}{R} = k_0 \tan\left(\frac{\pi}{2} - \gamma^n\right) \approx k_0 \sin\left(\frac{\pi}{2} - \gamma^n\right) = k_0 \cos \gamma^n,$$

where  $\gamma^n$  is the angle between the platform velocity and the direction from  $\mathbf{x}^n$  to the target  $\mathbf{z}$ ; see Figure 1. For narrow antenna beams and broadside imaging, the angle  $\frac{\pi}{2} - \gamma^n$  is small, which is why the approximation in (A.8) holds. Using (A.8), we can rewrite (A.7) as

$$(A.9) \quad W_A(\mathbf{y}, \mathbf{z}) = \sum_{n=-N/2}^{N/2} e^{2ik_0 \cos \gamma^n (y_1-z_1)} = \sum_{n=-N/2}^{N/2} e^{2i\omega_0 \cos \gamma^n (y_1-z_1)/c},$$

which shows that the variation of the local wavenumber along the synthetic array can be attributed to a Doppler-like effect. Indeed, it is well known that the standard linear Doppler frequency shift is proportional to the ratio of the platform speed over the wave propagation speed times the cosine of the angle between the platform velocity and the direction to the target:

$$\omega - \omega_0 \propto \frac{v}{c} \cos \gamma.$$

In (A.9), the actual physical Doppler effect, which is due to the platform motion, does not manifest itself, because we are using the start-stop approximation, and the platform is considered motionless at the times when it emits and receives the SAR signals.<sup>13</sup> On the other

---

<sup>13</sup>The role of the platform motion and the corresponding Doppler effect in SAR analysis is discussed in detail in [30].

hand, it is common to associate the change in the antenna position, i.e., the variation of  $n$ , with the so-called slow time; see, e.g., [6, Chapter 9]. Then, the local wavenumber  $k(n)$  can be thought of as a function of slow time. The dependence of  $k(n)$  on slow time is through  $\cos \gamma^n$ , so that its value is determined by the transmitting/receiving location  $n$  only and is not affected by how rapidly the platform moves between different locations. Thus, the quantity  $\cos \gamma^n$  in the exponent in formula (A.9) can be interpreted as the second contributing factor to the Doppler frequency shift in slow time. This frequency (or wavenumber) shift varies linearly along the synthetic array, which can also be seen as a chirp in the azimuthal direction. It is to be noted, though, that in the literature the Doppler interpretation of synthetic arrays is sometimes artificially attributed to the physical fast time  $t$ , as opposed to the slow time  $n$ ; see, e.g., [7, section 3.5.5] or [12, section 1.4.2.2].

**Appendix B. Leontovich boundary condition.** An alternative scattering model that is simpler than that of section 3 yet capable of producing similar results, albeit with less mathematical rigor, is the model based on impedance boundary conditions [25], i.e., boundary conditions of the third kind. A particular form of such boundary conditions that will be of interest for our analysis corresponds to an interface with a large jump of the refractive index:  $\varepsilon^{(0)} \gg 1$ . In this case, the refracted wave propagates almost normal to the interface regardless of the angle of incidence. This allows one to establish an approximate relation between the total field and its normal derivative on the vacuum side of the interface, thus removing the material domain from consideration. In the literature, this relation is often referred to as the Leontovich (or Shchukin–Leontovich) boundary condition; see [1, 24, 31].

Consider a solution  $u = u(z_1, z_2, z_3)$  to the pair of Helmholtz equations (3.6). It is a wave field with the spatial frequency  $k$  in the upper half-space ( $z_3 > 0$ ) and  $k' = k\sqrt{\varepsilon^{(0)}}$  in the lower half-space ( $z_3 < 0$ ). Suppose also that, similarly to (3.5),

$$u = \begin{cases} u_i + u_r, & z_3 > 0, \\ u_t, & z_3 < 0, \end{cases}$$

where  $u_i$ ,  $u_r$ , and  $u_t$  are the incident, reflected, and transmitted fields, respectively. Let

$$\hat{u} = \hat{u}(\zeta_1, \zeta_2, z_3) = \frac{1}{(2\pi)^2} \iint u(z_1, z_2, z_3) e^{-i(\zeta_1 z_1 + \zeta_2 z_2)} dz_1 dz_2.$$

Then, we can write

$$(B.1) \quad \hat{u} = \begin{cases} u_i e^{-iqz_3} + u_r e^{iqz_3}, & z_3 > 0, \\ u_t e^{-iq'z_3}, & z_3 < 0, \end{cases}$$

where  $u_i$ ,  $u_r$ , and  $u_t$  are amplitudes that depend on the Fourier variables  $(\zeta_1, \zeta_2)$ ,  $q^2 = k^2 - \zeta_1^2 - \zeta_2^2$ , and  $q'^2 = k'^2 - \zeta_1^2 - \zeta_2^2$ . The transmitted/reflected part of solution (B.1) satisfies radiation boundary conditions as  $z_3 \rightarrow \infty$  and  $z_3 \rightarrow -\infty$ . Moreover, as in section 3, we are assuming that the overall solution  $u$  and its normal derivative  $\frac{\partial u}{\partial z_3}$  are continuous at  $z_3 = 0$ . This yields (cf. (3.11))

$$\begin{aligned} u_i + u_r &= u_t, \\ -iq u_i + iq u_r &= -iq' u_t. \end{aligned}$$

Consequently,

$$\frac{1}{\hat{u}} \frac{\partial \hat{u}}{\partial z_3} \Big|_{z_3=+0} = \frac{-iq \mathbf{u}_i + iq \mathbf{u}_r}{\mathbf{u}_i + \mathbf{u}_r} = \frac{-iq' \mathbf{u}_t}{\mathbf{u}_t} = -iq'$$

or

$$(B.2) \quad \frac{\partial \hat{u}}{\partial z_3} \Big|_{z_3=+0} = -iq' \hat{u} \Big|_{z_3=+0} = -i \sqrt{\varepsilon^{(0)} k^2 - \zeta_1^2 - \zeta_2^2} \hat{u} \Big|_{z_3=+0}.$$

Using (B.2), for the normal derivative of the overall solution  $u(z_1, z_2, z_3)$  in the physical (as opposed to Fourier) variables we have

$$(B.3) \quad \begin{aligned} \frac{\partial u}{\partial z_3} \Big|_{z_3=+0} &= \frac{1}{(2\pi)^2} \iint -i \sqrt{\varepsilon^{(0)} k^2 - \zeta_1^2 - \zeta_2^2} \hat{u}(\zeta_1, \zeta_2, 0) e^{i(\zeta_1 z_1 + \zeta_2 z_2)} d\zeta_1 d\zeta_2 \\ &= \frac{-i}{(2\pi)^2} \iint \sqrt{\varepsilon^{(0)} k^2 - \zeta_1^2 - \zeta_2^2} e^{i(\zeta_1 z_1 + \zeta_2 z_2)} \iint u(z'_1, z'_2, 0) e^{-i(\zeta_1 z'_1 + \zeta_2 z'_2)} dz'_1 dz'_2 d\zeta_1 d\zeta_2 \\ &= \frac{-i}{(2\pi)^2} \iint u(z'_1, z'_2, 0) \iint \sqrt{\varepsilon^{(0)} k^2 - \zeta_1^2 - \zeta_2^2} e^{i(\zeta_1(z_1 - z'_1) + \zeta_2(z_2 - z'_2))} d\zeta_1 d\zeta_2 dz'_1 dz'_2, \end{aligned}$$

which is a nonlocal relation between  $u$  and its normal derivative at  $z_3 = 0$ . The nonlocal nature of this and similar relations is well known; see, e.g., [28]. However, for large  $\varepsilon^{(0)}$  relation (B.3) can be approximately localized. Indeed, if  $\varepsilon^{(0)} \gg 1$ , instead of (B.2) we can write

$$(B.4) \quad \frac{\partial \hat{u}}{\partial z_3} \Big|_{z_3=+0} = -i \sqrt{\varepsilon^{(0)} k^2 - \zeta_1^2 - \zeta_2^2} \hat{u} \Big|_{z_3=+0} \approx -ik \sqrt{\varepsilon^{(0)}} \hat{u} \Big|_{z_3=+0},$$

where the right-hand side no longer depends on  $(\zeta_1, \zeta_2)$ . It is important to realize, though, that this approximation cannot be directly used in (B.3). Indeed, the integration  $d\zeta_1 d\zeta_2$  in (B.3) is performed over the entire plane, and approximation (B.4) obviously does not hold for all  $(\zeta_1, \zeta_2)$ . To be able to substitute (B.4) into (B.3), we first need to require that the Fourier transform  $\hat{u}(\zeta_1, \zeta_2, 0)$  decay sufficiently rapidly as  $\zeta_1^2 + \zeta_2^2 \rightarrow \infty$ , so that the contribution of those Fourier components, for which (B.4) does not hold, can be neglected. This requirement is equivalent to a certain degree of smoothness of  $u(z_1, z_2, 0)$ , but in this paper we will not attempt to accurately quantify either the required rate of decay of  $\hat{u}(\zeta_1, \zeta_2, 0)$  or the equivalent level of regularity of  $u(z_1, z_2, 0)$ . We will merely assume that (B.4) can be used.

Once (B.4) is substituted into (B.3), the interior double integral on the last line of (B.3) evaluates to  $-ik \sqrt{\varepsilon^{(0)}} \delta(z_1 - z'_1, z_2 - z'_2)$ , which yields a local relation between the solution and its normal derivative in physical variables:

$$(B.5) \quad \frac{\partial u}{\partial z_3} \Big|_{z_3=+0} = -ik \sqrt{\varepsilon^{(0)}} u \Big|_{z_3=+0}.$$

Relation (B.5) is the Leontovich boundary condition.

Next, we generalize boundary condition (B.5) by allowing the permittivity to vary:

$$(B.6) \quad \left. \frac{\partial u}{\partial z_3} \right|_{z_3=+0} = -ik\sqrt{\varepsilon}u \Big|_{z_3=+0}.$$

We emphasize that (B.6) is only a formal extension of (B.5) to the case of a variable permittivity. It cannot be derived using the same Fourier approach as we used for obtaining (B.5). The motivation for introducing (B.6) is rather qualitative: as in the case of a constant permittivity, all the refracted waves propagate close to normal, and the same will roughly be true for variable permittivity, as long as this permittivity remains large.

Having introduced (B.6), we assume as in section 3 that  $u = u^{(0)} + u^{(1)}$  and  $\varepsilon = \varepsilon^{(0)} + \varepsilon^{(1)}$ , and we apply the method of perturbations. In doing so, we also assume that the incident field is a plane wave propagating at an angle  $\theta$ ; see (3.1). Then, for zero order, (B.6) yields

$$-iq_i \mathbf{u}_i^{(0)} + iq_i \mathbf{u}_r^{(0)} = -ik\sqrt{\varepsilon^{(0)}}(\mathbf{u}_i^{(0)} + \mathbf{u}_r^{(0)}),$$

where  $q_i = k \cos \theta$ . Hence, we obtain the following zero order reflection coefficient:

$$(B.7) \quad \frac{\mathbf{u}_r^{(0)}}{\mathbf{u}_i^{(0)}} = -\frac{k\sqrt{\varepsilon^{(0)}} - q_i}{k\sqrt{\varepsilon^{(0)}} + q_i} = -\frac{\sqrt{\varepsilon^{(0)}} - \cos \theta}{\sqrt{\varepsilon^{(0)}} + \cos \theta}.$$

This reflection coefficient approximately coincides with that of (3.12) if we assume in (3.12) that  $\cos \theta' \approx 1$ , which is consistent with the near normal propagation of the refracted waves.

For first order perturbations, from boundary condition (B.6) we derive

$$\left. \frac{\partial u^{(1)}}{\partial z_3} \right|_{z_3=+0} = -ik\sqrt{\varepsilon^{(0)}} \left( u^{(1)} + \frac{\varepsilon^{(1)}}{2\varepsilon^{(0)}} u^{(0)} \right) \Big|_{z_3=+0}.$$

Then, assuming as in (3.16) that  $\hat{u}^{(1)} = \mathbf{u}_i^{(0)} \mathbf{b} e^{iqz_3}$  for  $z_3 > 0$ , we get

$$iq\mathbf{u}_i^{(0)} \mathbf{b} = -ik\sqrt{\varepsilon^{(0)}} \left[ \mathbf{u}_i^{(0)} \mathbf{b} + \frac{\hat{\varepsilon}_\theta}{2\varepsilon^{(0)}} (\mathbf{u}_i^{(0)} + \mathbf{u}_r^{(0)}) \right],$$

where  $\hat{\varepsilon}_\theta = \hat{\varepsilon}^{(1)}(\zeta_1, \zeta_2 - k \sin \theta)$  is introduced in (3.15). This expression along with (B.7) yields

$$(B.8) \quad \mathbf{b} = -\frac{\hat{\varepsilon}_\theta}{\sqrt{\varepsilon^{(0)}}} \frac{kq_i}{(k\sqrt{\varepsilon^{(0)}} + q)(k\sqrt{\varepsilon^{(0)}} + q_i)}.$$

Similarly to zero order, the first order reflection coefficient  $\mathbf{b}$  of (B.8) approximately coincides with that of (3.22) if in (3.22) we assume that  $q'_r = k' \cos \theta' \approx k' = k\sqrt{\varepsilon^{(0)}}$  and also that  $q' \approx q'_r$ , because the propagation in the material is almost normal anyway. The new form of  $\mathbf{b}$  given by (B.8) will affect  $\mathcal{M}$  of (3.33), but the rest of the analysis will stay unaltered.

## REFERENCES

- [1] F. G. BASS AND I. M. FUKS, *Wave Scattering from Statistically Rough Surfaces*, Pergamon Press, Oxford, New York, 1979 (translated and edited by C. B. Vesecky and J. F. Vesecky).
- [2] E. BLESZYNSKI, M. BLESZYNSKI, AND T. JAROSZEWICZ, *Autofocus algorithm for synthetic aperture radar imaging with large curvilinear apertures*, *Inverse Problems*, 29 (2013), 054004.
- [3] M. BORN AND E. WOLF, *Principles of optics: Electromagnetic theory of propagation, interference and diffraction of light*, 7th ed., with contributions by A. B. Bhatia, P. C. Clemmow, D. Gabor, A. R. Stokes, A. M. Taylor, P. A. Wayman, and W. L. Wilcock, Cambridge University Press, Cambridge, UK, 1999.
- [4] F. CAKONI, D. COLTON, AND P. MONK, *The Linear Sampling Method in Inverse Electromagnetic Scattering*, CBMS-NSF Regional Conf. Ser. in Appl. Math. 80, SIAM, Philadelphia, 2011.
- [5] M. CHENEY, *A mathematical tutorial on synthetic aperture radar*, *SIAM Rev.*, 43 (2001), pp. 301–312.
- [6] M. CHENEY AND B. BORDEN, *Fundamentals of Radar Imaging*, CBMS-NSF Regional Conf. Ser. in Appl. Math. 79, SIAM, Philadelphia, 2009.
- [7] I. G. CUMMING AND F. H. WONG, *Digital Processing of Synthetic Aperture Radar Data. Algorithms and Implementation*, Artech House, Boston, 2005.
- [8] L. J. CUTRONA, *Synthetic aperture radar*, in *Radar Handbook*, 2nd ed., M. Skolnik, ed., McGraw–Hill, New York, 1990, Chapter 21.
- [9] M. V. FEDORYUK, *The Saddle-Point Method [Metod perevala]*, Nauka, Moscow, 1977 (in Russian).
- [10] J.-P. FOUQUE, J. GARNIER, G. PAPANICOLAOU, AND K. SØLNA, *Wave Propagation and Time Reversal in Randomly Layered Media*, *Stoch. Model. Appl. Probab.* 56, Springer, New York, 2007.
- [11] J.-P. FOUQUE AND O. V. POLIANNIKOV, *Time reversal detection in one-dimensional random media*, *Inverse Problems*, 22 (2006), pp. 903–922.
- [12] G. FRANCESCHETTI AND R. LANARI, *Synthetic Aperture Radar Processing*, Electronic Engineering Systems Series, CRC Press, Boca Raton, FL, 1999.
- [13] M. GILMAN, E. SMITH, AND S. TSYNKOV, *A linearized inverse scattering problem for the polarized waves and anisotropic targets*, *Inverse Problems*, 28 (2012), 085009.
- [14] M. GILMAN, E. SMITH, AND S. TSYNKOV, *Reduction of ionospheric distortions for spaceborne synthetic aperture radar with the help of image registration*, *Inverse Problems*, 29 (2013), 054005.
- [15] M. GILMAN, E. SMITH, AND S. TSYNKOV, *Single-polarization SAR imaging in the presence of Faraday rotation*, *Inverse Problems*, 30 (2014), 075002.
- [16] M. GILMAN, E. SMITH, AND S. TSYNKOV, *Transionospheric Synthetic Aperture Imaging*, Birkhäuser, New York, 2015, to appear.
- [17] K. HASSELMANN, R. K. RANEY, W. J. PLANT, W. ALPERS, R. A. SHUCHMAN, D. R. LYZENGA, C. L. RUFENACH, AND M. J. TUCKER, *Theory of synthetic aperture radar ocean imaging: A MARSEN view*, *J. Geophys. Res. Oceans*, 90 (1985), pp. 4659–4686.
- [18] G. KAISER, *A Friendly Guide to Wavelets*, Birkhäuser Boston, Boston, MA, 1994.
- [19] A. KIRSCH AND N. GRINBERG, *The Factorization Method for Inverse Problems*, Oxford Lecture Ser. Math. Appl. 36, Oxford University Press, Oxford, 2008.
- [20] L. D. LANDAU AND E. M. LIFSHITZ, *Course of Theoretical Physics, Vol. 2, The Classical Theory of Fields*, 4th ed., Pergamon Press, Oxford, 1975 (translated from the Russian by M. Hamermesh).
- [21] F. C. LIN AND M. A. FIDDY, *The Born-Rytov controversy: I. Comparing analytical and approximate expressions for the one-dimensional deterministic case*, *J. Opt. Soc. Amer. A*, 9 (1992), pp. 1102–1110.
- [22] D. L. MARKS, *A family of approximations spanning the Born and Rytov scattering series*, *Opt. Express*, 14 (2006), pp. 8837–8848.
- [23] L. J. MOORE AND L. C. POTTER, *Three-dimensional resolution for circular synthetic aperture radar*, in *Defense and Security Symposium*, SPIE, Bellingham, WA, 2007, 656804.
- [24] G. PELOSI AND P. YA. UFIMTSEV, *The impedance-boundary condition*, *IEEE Trans. Antennas and Propagation*, 38 (1996), pp. 31–35.
- [25] T. B. A. SENIOR AND J. L. VOLAKIS, *Approximate Boundary Conditions in Electromagnetics*, IEEE Electromagnetic Waves Ser. 41, IEEE Press, London, 1995.
- [26] E. M. SMITH AND S. V. TSYNKOV, *Dual carrier probing for spaceborne SAR imaging*, *SIAM J. Imaging Sci.*, 4 (2011), pp. 501–542.

- [27] P. SOTIRELIS, J. PARKER, X. HU, M. CHENEY, AND M. FERRARA, *Frequency-dependent reflectivity image reconstruction*, in SPIE Defense, Security, and Sensing, SPIE, Bellingham, WA, 2013, 874602.
- [28] S. V. TSYNKOV, *Numerical solution of problems on unbounded domains. A review*, Appl. Numer. Math., 27 (1998), pp. 465–532.
- [29] S. V. TSYNKOV, *On SAR imaging through the Earth's ionosphere*, SIAM J. Imaging Sci., 2 (2009), pp. 140–182.
- [30] S. V. TSYNKOV, *On the use of start-stop approximation for spaceborne SAR imaging*, SIAM J. Imaging Sci., 2 (2009), pp. 646–669.
- [31] A. VORONOVICH, *Wave Scattering from Rough Surfaces*, Springer, Berlin, 1999.